MULTI-SCALE CONTROL AND ENHANCEMENT OF REACTOR BOILING HEAT FLUX BY REAGENTS AND NANOPARTICLES

R. M. Manglik, A. Athavale, D. S. Kalaikadal,
A. Deodhar, and U. Verma

August 2011

Final Technical Report TFTPL-21-DOE-NEER

[PROJECT TITLE: Reactor Engineering: Multi-Scale Control & Enhancement of Reactor Boiling Heat Flux by Reagents and Nanoparticles]

Final Technical Report submitted to:
U.S. Department of Energy
NEER Grant No. **DE-FG07-07ID14772**
May 01, 2007 - Apr 30, 2011

Thermal-Fluids & Thermal Processing Laboratory

Department of Mechanical, Industrial & Nuclear Engineering
University Of Cincinnati
Cincinnati, Ohio 45221-0072

ACKNOWLEDGEMENTS

The compilation and reporting of this work was supported in part by a grant (No. DE-FG07-07ID14772) from the US Department of Energy (DOE) under the Nuclear Energy Education Research (NEER) program. Additional support and facilities were provided by the Thermal-Fluids & Thermal Processing Laboratory, the National Science Foundation, and the Mechanical, Industrial and Nuclear Engineering Department, University of Cincinnati. Also, the extended discussions with Professors Milind A. Jog, Jude Iroh, and Y.-K. Kao, and their advice during the term of this project are gratefully acknowledged. Laboratory assistance was also provided by R. Bhatia, G. B. Wickizer, V. Ravi, A. Subramani, S. K. Kasimsetty, and S. C. Vishnubhatla.

ABSTRACT

The phenomenological characterization of the use of non-invasive and passive techniques to enhance the boiling heat transfer in water has been carried out in this extended study. It provides fundamental enhanced heat transfer data for nucleate boiling and discusses the associated physics with the aim of addressing future and next-generation reactor thermal-hydraulic management. It essentially addresses the hypothesis that in phase-change processes during boiling, the primary mechanisms can be related to the liquid-vapor interfacial tension and surface wetting at the solid-liquid interface. These interfacial characteristics can be significantly altered and decoupled by introducing small quantities of additives in water, such as surface-active polymers, surfactants, and nanoparticles. The changes are fundamentally caused at a *molecular-scale* by the relative bulk molecular dynamics and adsorption-desorption of the additive at the liquid-vapor interface, and its physisorption and electrokinetics at the liquid-solid interface. At the *micro-scale*, the transient transport mechanisms at the solid-liquid-vapor interface during nucleation and bubble-growth can be attributed to thin-film spreading, surface-micro-cavity activation, and micro-layer evaporation. Furthermore at the *macro-scale*, the heat transport is in turn governed by the bubble growth and distribution, macro-layer heat transfer, bubble dynamics (bubble coalescence, collapse, break-up, and translation), and liquid rheology. Some of these behaviors and processes are measured and characterized in this study, the outcomes of which advance the concomitant fundamental physics, as well as provide insights for developing control strategies for the molecular-scale manipulation of interfacial tension and surface wetting in boiling by means of polymeric reagents, surfactants, and other soluble surface-active additives.

This DOE-NEER study has three prominent parts to the investigation, namely, (a) interfacial characterization of aqueous reagent solutions, (b) bubble dynamics in isothermal liquid pools, and (c) nucleate boiling in aqueous polymeric and surfactant-laden solutions. The present report, while summarizing the outcomes of the entire DOE-NEER study, gives extended details of the boiling experiments as well as discusses the results thereof (part (c)). Prominent aspects of part (b) are also discussed, while the work of part (a) is embedded in that of part (c) reported here; two previous reports [1, 2] document more details for parts (a) and (b) of this work.

TABLE OF CONTENTS

LIST OF ARCHIVAL PAPERS

List of papers published or in press:

- R.M. Manglik, Molecular-to-macro-scale control of interfacial behavior in ebullient phase change in aqueous solutions of reagents, *International Journal of Transport Phenomena*, **12**, 2011 (in press).
- A.D. Athavale, R.M. Manglik, and M.A. Jog, An experimental investigation of nucleate pool boiling in aqueous solutions of a polymer, *AIChE Journal*, 2011 (in press; DOI: 10.1002/aic.12616).
- U. Verma, R.M. Manglik, and M.A. Jog, Experimental study of effects of interfacial properties on nucleate pool boiling in water, *Proc. ASME – IMECE 2011*, Denver, CO, Paper No. IMECE2011-62740, Nov 2011.
- R.M. Manglik, Interfacial phenomena in nucleate pool boiling of water: their role and manipulation by molecular dynamics of surface-active additives, *Proc. 9th International ISHMT-ASME Conference*, Mumbai, India, January 2010.
- R.M. Manglik and M.A. Jog, Molecular-to-large-scale heat transfer with multiphase interfaces: current status and new directions, *Journal of Heat Transfer*, **131**(12), 121001(1-11), 2009.
- A. Subramani, M.A. Jog, and R.M. Manglik, Air-water ebullience systems: visualizing single bubble to wave instability signatures, *Journal of Heat Transfer*, **130**(8), 080905-1, 2008.

List of papers in preparation or submitted for review:

- D.S. Kalaikadal, S.K. Kasimsetty, and R.M. Manglik, A theoretical model for gas-bubble growth at a submerged capillary-tube orifice tip in quiescent liquid pools, *Chemical Engineering Science*, 2011.
- A. Athavale and R. M. Manglik, Pseudoplasticity and dynamic interfacial effects on nucleate boiling in polymeric liquids, *International Journal of Multiphase Flow*, 2011.
- R.M. Manglik and A. Subramani, Visualization and characterization of dynamics of gas bubbles from capillary-tube orifices in a liquid pool: growth, departure, and coalescence, *Experimental Thermal and Fluid Science*, 2011.
- R.M. Manglik, S.C. Vishnubhatla, R. Gupta, V. Ravi, and A. Athavale, Interfacial and rheological characterization of aqueous solutions of surfactants and polymeric reagents, *Colloid and Interface Science*, 2011.

MOLECULAR-TO-MACRO-SCALE CONTROL OF INTERFACIAL BEHAVIOR IN EBULLIENT PHASE CHANGE IN AQUEOUS SOLUTIONS OF REAGENTS

Introduction

Nucleate boiling has found increasingly new applications because considerably high heat transfer rates can be sustained in the liquid-vapor phase-change process with relatively small driving temperature differences. In fact, it is encountered in a wide spectrum of engineering systems of different spatial scales (very large to very small) that include, among others, energy conversion, refrigeration and air-conditioning, chemical thermal processing, heat treatment and manufacturing, microelectronic cooling, and numerous emerging miniaturized devices (MEMS, MTMS, μ-TAS, micro heat pipes, lab-on-chips, etc.). The attendant research that has attempted to unravel many fundamental as well as applied issues has spanned more that two centuries [3-6], and the current imperatives for sustainable energy consumption and production are expected to add new dimensions to this work [5].

While mechanistically characterizing the phase-change process in nucleate boiling is quite complex [5, 7-10], a set of primary controls and determinants can essentially be related to the transient *micro-scale* transport mechanisms at the solid-liquid-vapor interface schematically depicted in Fig. 1. For instance, the surface wetting at the liquid-solid interface influences micro-cavity activation, nucleation of embryonic vapor bubbles, thin-film spreading, and micro-layer evaporation [11-16]. Similarly, the changing liquid-vapor interface is affected by the surface tension behavior that determines post-nucleation bubble dynamics (bubble size, shape, frequency, coalescence, break-up, and translation) and lends to Marangoni flow or micro-convection [9, 17-20]. In the post-departure bubble dynamics, besides the interfacial tension, the

shear forces at the liquid-vapor interface characterized by liquid viscosity or rheology also play a role [14, 21, 22].

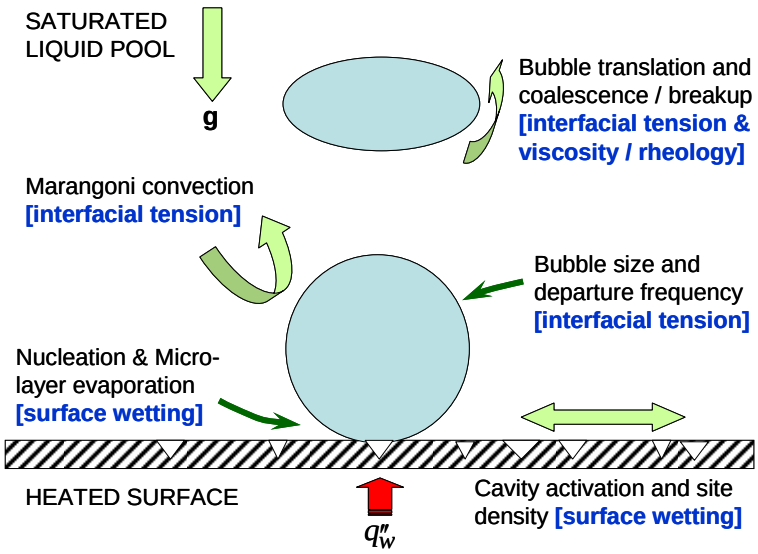

Figure 1. Schematic representation of the impact of liquid-vapor-solid interfacial properties on ebullient dynamics in saturated nucleate pool boiling.

The ability to passively control surface wetting (liquid-solid interface) and dynamical interfacial tension at the liquid-vapor interface is attractively offered by the *molecular-scale* adsorption-physisorption dynamics and electrokinetics of surface-active additives or reagents, such as surfactants, polymers, soluble nanoparticles, etc. [21, 23-26]. In pure liquids, interfacial or surface tension and wetting are conjoined, i.e., a low surface tension liquid has high wetting and vice versa. By adding reagents in water, however, and depending upon their molecular structure and electrokinetics, these two interfacial properties can be passively decoupled to the extent that low surface tension and yet low wetting can manifest [25, 27-30]. Such a control strategy has revolutionary implications for thermal management by nucleate boiling in a diverse spectrum of applications that range from micro-scale devices to large-scale terrestrial and space-based heat exchange systems.

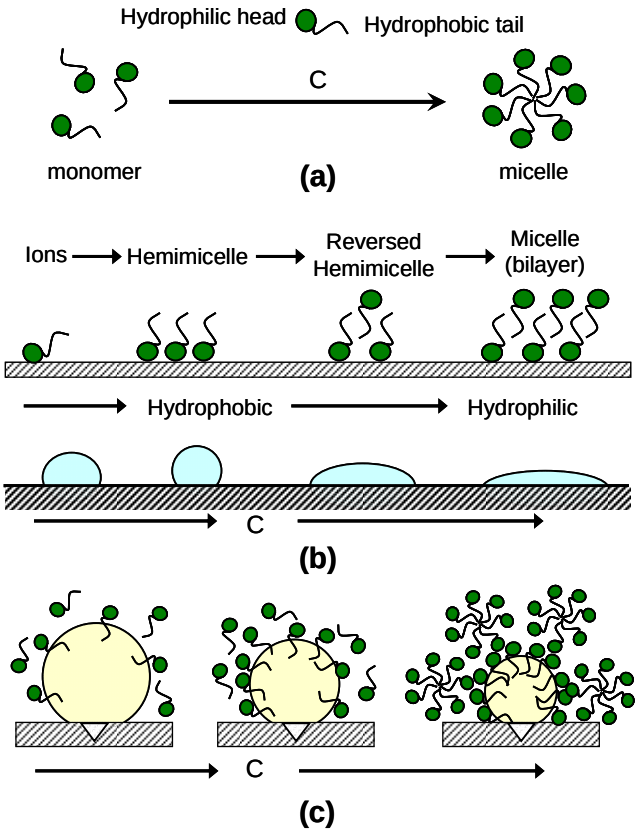

Figure 2. Reagent-dynamics-based interfacial phenomena in aqueous surfactant solutions: (a) surfactant molecule and concentration-based structure, (b) physisorption at solid-liquid interface, and (c) adsorption at liquid-vapor interface.

Reagent Molecular Dynamics

A variety of different surface-active agents (surfactants, polymers, electrolytes, etc.) can be added in small concentrations to alter the interfacial properties of liquids [5, 6, 26, 31-34]. Among these, surfactants are particularly effective additives as they have a unique long-chain molecular structure composed of a hydrophilic head and a hydrophobic tail (Fig. 2a) [27, 33]. Based on the nature of the hydrophilic part of the molecule that is ionizable, polar, and polarizable, surfactants are generally categorized as anionics, nonionics, cationics, and zwitterionics [33]. They all have a natural tendency to adsorb at surfaces and interfaces when added in water, and, depending upon the reagent concentration, their solution forms an

association colloid where the reagent molecules form aggregates or micelles; the concentration at which this occurs is referred to as the critical micelle concentration or CMC. When nucleate boiling or ebullient phase-change occurs in such solutions, the reagent molecular dynamics significantly alters the interfacial properties in the vicinity of a forming and translating bubble that are schematically highlighted in Fig. 1.

The dynamic surfactant-concentration-based changes that can be incurred at the two primary interfaces in the ebullient phase-change process are illustrated in Fig. 2(b)-(c), and can be summarized as follows:

(1) Surfactant adsorption-desorption at the vapor-liquid interface alters the interfacial or surface tension, which decreases continually with increasing concentrations till the critical micelle concentration or CMC is attained. This interfacial tension relaxation is caused by both a diffusion-rate-dependent and a surface-age- or time-dependent process. They are typically affected by the type of surfactant, its diffusion-adsorption or molecular kinetics, micellar dynamics, level of ethoxylation, and bulk concentration in solution [33, 35, 36].

(2) The physisorption of surfactant molecules at the solid-liquid interface changes the surface wetting behavior. With increasing concentration, in many aqueous surfactant solutions, the resulting adsorption behavior and surface state can be categorized into four different regimes [30]: (a) low-concentration adsorption as individual ions ; (b) sharp increase in the adsorption density due to self-association of adsorbed surfactant ions and the formation of hemimicelles; (c) adsorption as reverse hemimicelles, with their polar heads oriented both toward the surface and liquid, to render the surface increasingly hydrophilic; and (d) as the CMC is approached, the adsorption becomes independent of

the bulk concentration, and the surfactant molecules form a bilayer on the surface to make it strongly hydrophilic.

Furthermore, and as also pointed out by Hoffmann and Rehage [37] and observed in some recent experimental studies [23-25], dilute solutions of both ionic and nonionic surfactants usually behave as Newtonian liquids, and their viscosity is generally close to that of the solvent.

In the case of polymeric additives, on the other hand, the solvent viscosity can increase substantially. Most polymers are large molecules, macromolecules, or agglomerates of smaller chemical units called monomers, and are broadly classified as biological or non-biological macromolecules. The higher viscosity of their aqueous solution tends to increase with concentration as well as the molecular weight of the polymer, and often displays a shear-rate-dependent rheology [38, 39]. With the exception of some surface-active polymers (or polymeric surfactants) such as hydroxyl-ethyl cellulose (HEC) and polyethylene oxide (PEO), most polymer solutions do not show any significant change in surface tension σ [21, 35, 40]. The viscosity of the polymer solution, however, can considerably influence the measurement of surface tension, especially in higher viscosity solutions and at higher bubble frequency [21, 35, 41].

Surface tension relaxation in reagent-laden aqueous solutions is largely brought about by the molecular adsorption of the additives to the vapor-liquid interface [25, 27, 33, 42]. The time scales of this process vary from order of seconds to minutes, depending upon the surfactant (or polymer, or electrolyte) chemistry (as described by molecular weight, ionic character, molecular structure, etc.), and its concentration in solution [27]. As a result of this transient molecular adsorption characteristic, which lends to temporal variations in surface tension and surface wetting, and the typical time scales of the order of 10-to-100 ms for boiling-bubble dynamics in

water [25, 43], a rather complex interfacial behavior manifests in ebullient phase-change heat transfer.

Gas-Liquid Interfacial Behavior

In an equilibrium solution of a surfactant, when the bulk is disturbed either by surface expansion or contraction, as in the case of nucleate boiling, reagent molecules naturally adsorb at the newly formed and expanding gas(vapor)-liquid interface; some desorption may also occur, depending upon their ionic and molecular structure. This is a transient two-step process [44]: (1) molecular exchange between the surface layer and sub-surface layer or sub-layer by adsorption-desorption, and (2) molecular exchange between the sub-layer and bulk solution by diffusion. The sub-surface is the "boundary layer" that separates the bulk fluid domain, where only diffusion occurs, and the domain where only adsorption-desorption occurs. This process primarily reduces interfacial tension, and its time-dependent nature manifests in a dynamic surface tension behavior at an evolving vapor-liquid interface of a bubble; a finite time is required for complete interfacial relaxation and to reach equilibrium.

As seen in Fig. 3, surface tension σ of aqueous solutions of different surfactant decreases with increasing concentrations till CMC, when the reagent molecules agglomerate to form micelles; with C $\geq$ CMC, σ remains unchanged. The adsorption behavior of all reagents changes significantly around their respective CMC, and the micellization is a property of each solute. Different shapes, sizes, and ionic orientation of micelles can be formed, depending upon the type of reagent, its packing, concentration, temperature, presence of other ions, and water-soluble organic compounds in the solution [27, 33, 43, 45]. Also, σ is temperature dependant, dictated by reagent adsorption-desorption behavior. This is evident form the data for $\sigma - C$ variations

graphed in Fig. 3 for the three surfactants, namely, anionic SDS, cationic CTAB, and non-ionic Triton X-305 [25, 43, 46] at bulk temperatures of 23°C and 80°C. While σ is generally lower at the higher temperature, in both cases, σ also decreases with increasing C and asymptotically attains a minimum constant beyond CMC.

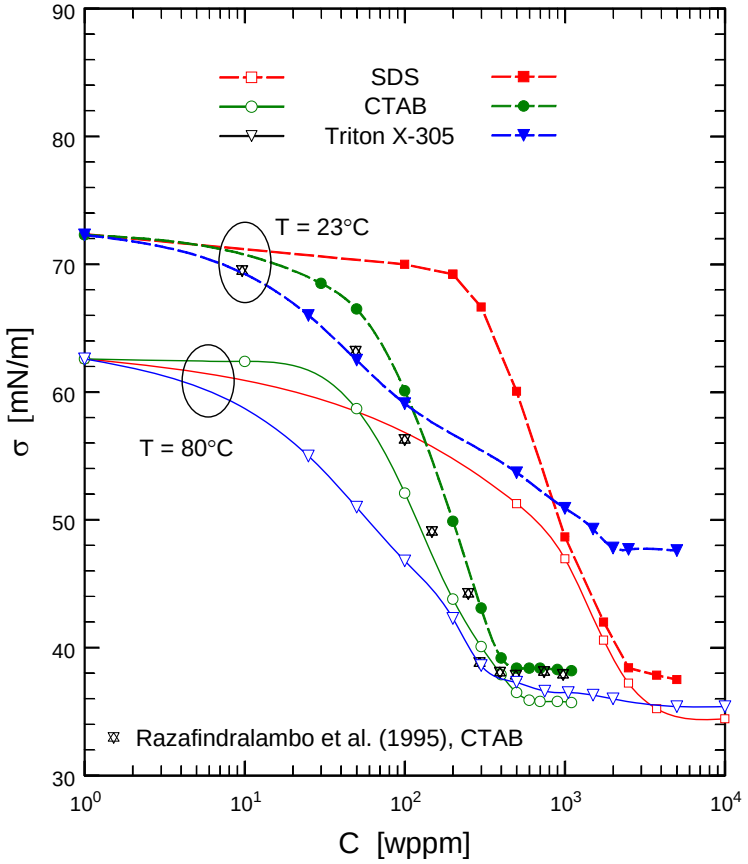

Figure 3. Variation of equilibrium interfacial tension σ with concentration C and bulk temperature in different aqueous surfactant solutions [25, 46].

Furthermore, the reagent adsorption at the newly created vapor-liquid interface of a nucleated and growing bubble is temporally characteristic. It requires a finite time period to attain an equilibrium condition between the adsorbed concentration at the interface and the bulk concentration. This gives rise to the dynamic surface tension (DST) behavior, or a $\sigma - \tau$

variation at a given bulk concentration where eventually the equilibrium interfacial tension relaxation is attained after a long time period [27, 35]. The data graphed in Fig. 4 clearly illustrates this fundamental characteristic. The time-dependent interfacial tension relaxation is also related to the molecular mobility of the reagent; a lower molecular mass surfactant diffuses faster than its higher molecular mass counterpart. All this gives credence to the contention that σ relaxation with time, or the DST, is perhaps the more critical determinant, instead of the equilibrium or static value, of the altered ebullience in nucleate boiling of reagent-laden aqueous solutions.

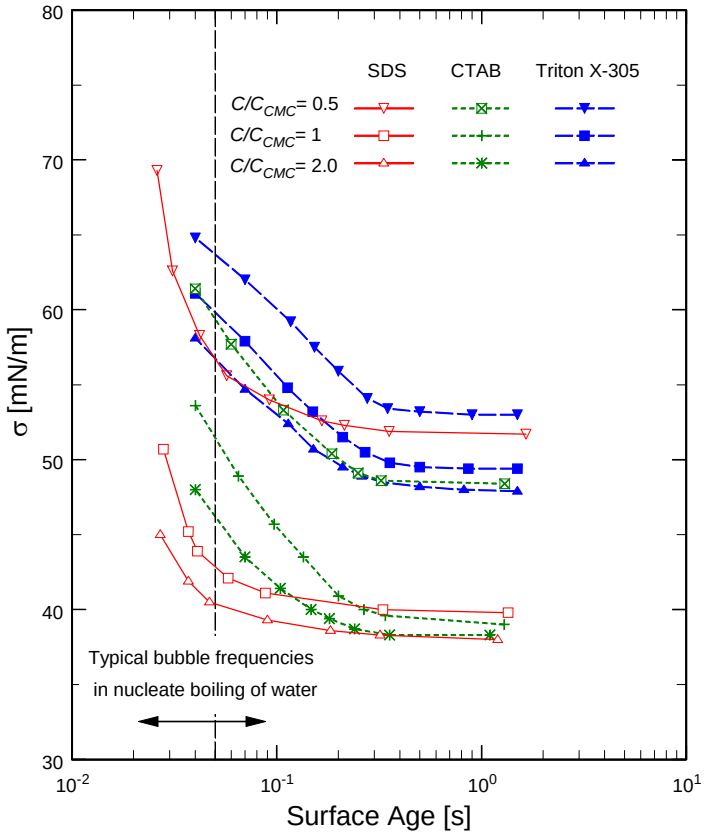

Figure 4. Time-dependent or dynamic surface tension behavior of aqueous surfactant solutions at room temperature (23°C; Zhang and Manglik, 2005a).

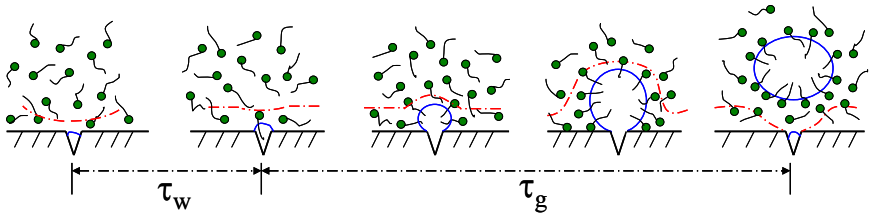

Figure 5. Reagent molecular transport at an evolving liquid-vapor bubble interface during nucleate boiling (not to scale).

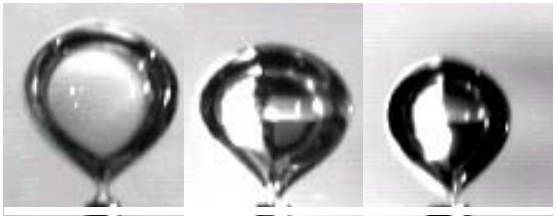

Figure 6. Dynamic surface tension effects on pre-departure shape and size of bubbles [43, 47].

The time scales for equilibrium at a new interface are typically of the order of 50 – 300 ms (see Fig. 4), whereas those for bubble formation and departure in nucleate boiling ~ 10 – 100 ms [19, 24, 43]. As a consequence of the $\sigma - \tau$ characteristic depicted by the data in Fig. 4, when a bubble starts to form at a nucleating site, the initial gas-liquid interfacial tension is or close to that of the solvent. It then reduces continually with τ as reagent molecules migrate to and adsorb at the interface; desorption may also occur at the evolving interface till an equilibrium condition is reached and surface tension becomes constant. This time-dependent adsorption-desorption around a nucleated and growing bubble is illustrated in Fig. 5. Additionally, DST effects on bubble formation and departure are demonstrated and clarified by the single-bubble experiment results of Fig. 6. Here a larger bubble is seen in aqueous SDS (sodium dodecyl sulfate) solution in comparison to that in a pure liquid (DMF or N,N-Dimenthyl Formamide), even though the two test fluids have the same bulk equilibrium σ value (~ 37 mN/m).

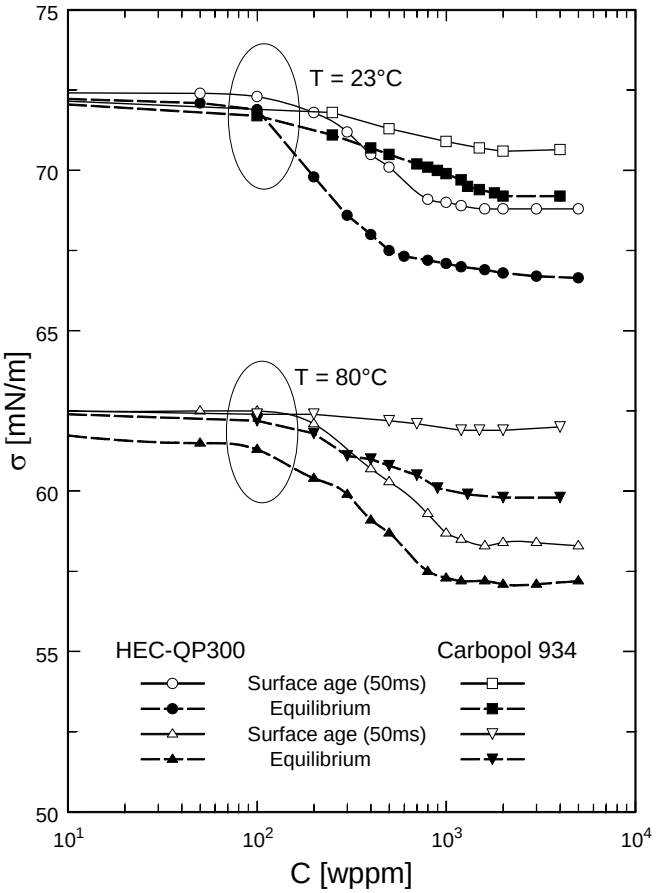

Figure 7. Equilibrium and dynamic surface tension data for aqueous HEC-QP300 and Carbopol 934 solutions [21].

Varying surface tension relaxation is also found in aqueous solutions of some types of polymer additives, as is evident from the data in Fig. 7 for different bubble frequencies and concentrations of HEC QP-300 and Carbopol 934. Furthermore, a critical polymer concentration, CPC or C_{cpc}, also known as the "overlap concentration," which is akin to the critical micelle concentration (CMC or C_{cmc}) in surfactant systems, is observed, such that σ relaxation attains a near constant value at or around C_{cpc} [21, 33, 48]. The nominal dynamic σ or DST, represented by the data for a bubble surface age of 50 ms, at both temperature conditions (23°C and 80°C) and at all $C > 0$, is seen to be greater than the corresponding equilibrium values for both HEC and Carbopol solutions. Also, the higher temperature results indicate overall

reduction in σ due to increased polymer diffusivity with increased temperature [33]. HEC solutions show significantly higher σ relaxation, relative to Carbopol solutions, both under dynamic and equilibrium conditions, with a rather sharp change in slope or surface tension gradient near C_{cpc}. This is because HEC is a surface-active polymer, and thus its adsorption behavior tends to be similar to those of surfactant solutions [33, 35]. Both equilibrium and dynamic σ values decrease with increasing concentration, and asymptotically become constant beyond C_{cpc}. Because of their molecular kinetics in water, in solutions with lower than overlap concentrations or C_{cpc}, the polymer molecules remain in the bulk solvent as isolated macromolecules with little intermolecular interactions. At overlap or "semi-dilute" concentrations, the polymer molecules "touch" each other, and, with increasing concentration, the frequency of collisions between the polymer coils eventually causes overlapping and entanglement of their chains.

Wetting and Electrokinetics

The reagent molecular physisorption at the solid-liquid interface or electrokinetics and micellar dynamics, as depicted in Fig. 2(b), alters surface wettability. This change with concentration, measured by the liquid-solid interface contact angle, is graphed in Fig. 8. Notably, ionic surfactants (anionic SDS and cationic CTAB) undergo a different adsorption process than that for nonionic surfactants (Triton X-305) due to the latter's lack of charge. The contact angle reaches a lower plateau around CMC where bilayers start to form on the surface. Nonionic surfactants, on the other hand, make the contact angle attain a constant value in solutions with concentrations much below CMC. In principle, direct interactions of their polar chain are generally weak, and it is possible for them to build and rebuild adsorption layers below

CMC [49]. The low contact angle trough at concentrations C < CMC can also be attributed to the absence of any electrical repulsion that could oppose molecular aggregation unlike that associated with ionic surfactants [50]. Furthermore, the continuous decrease in contact angle in solutions of nonionic Triton X-305 prior to reaching a constant value is brought about by the presence of 30 ethylene oxide (EO) groups in its molecular chain. The number of EO groups increases the overall size of the polar head, and controls the hydrophilic-hydrophobic balance on the surfactant molecule [33].

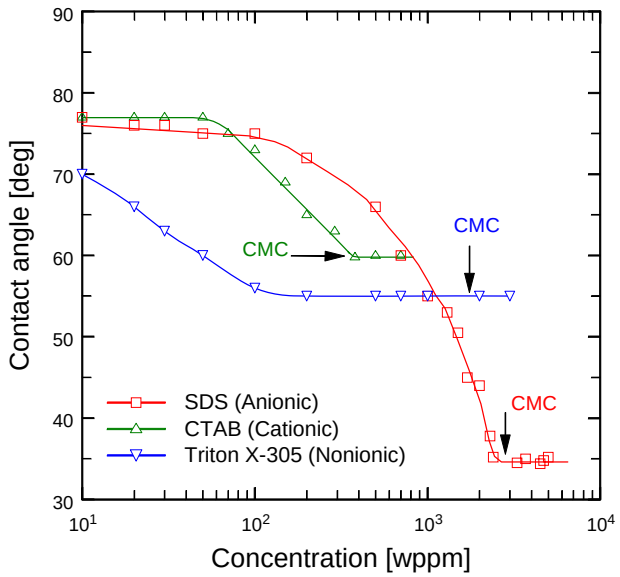

Figure 8. Variation of contact angle θ with concentration in different surfactant solutions [25].

Also displaying an increasing wetting behavior, different grades and anilide derivatives of polyethylene carboxylic acid (PEO or PE-CO2-OH) in aqueous solution show a remarkable change in the advancing contact angle θ_a or $\cos\theta_a$ (which is proportional to the interfacial free energy as governed by Young's equation) with the pH of the solution, as graphed in Fig. 9 [51]. Selective grades and derivatives of this polymer are seen to promote large hydrophobicity ($\theta >$ 90°) compared to others that contrastingly make the aqueous solutions more hydrophilic ($\theta <$

90°). Most interestingly the anilide derivatives (ortho, meta, and para) of PE-(ONH)-CO2H are seen (Fig. 9) to bring about dramatic changes in $\cos\theta_a$ – from large hydrophobicity to hydrophilicity – with varying pH of its water solution. This in essence provides a mechanism of controlling the solid-liquid interfacial tension or wettability, and delinking it from any changes in gas-liquid interfacial tension or surface tension.

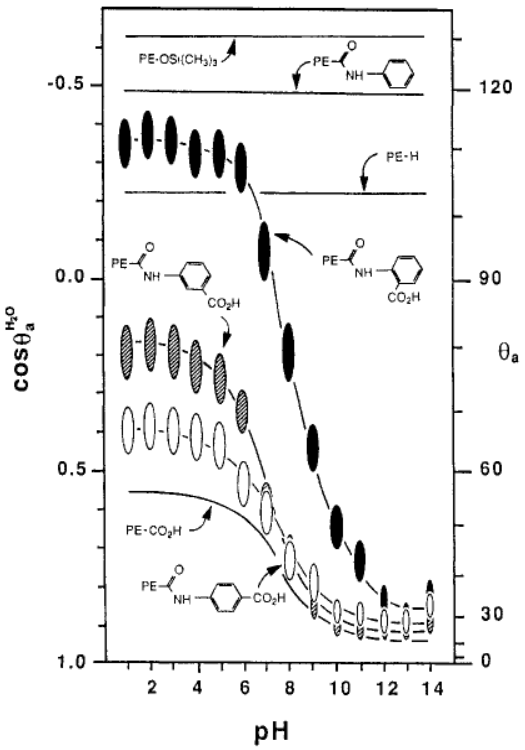

Figure 9. Variation of advancing contact angle $\cos\theta_a$ with pH in different water-polymer (anilide derivatives of PE-CO2-OH) solutions [51].

Furthermore, electrokinetic effects manifest when one phase is caused to move tangentially past another phase. In a colloidal system of finely dispersed reagent in solution, many different interfaces can exist, depending upon which state (gas, liquid, or solid) is finely dispersed in another [36], and the interaction between two phases generally develops a potential difference between them. With the presence of ions, or excess electrons, or ionogenic groups in one or both

phases, there is a tendency for the electric charges to distribute themselves in a particular direction at the interface [36, 52, 53]. An electrokinetic boundary layer, or an electric double layer (EDL), develops when a solid surface containing immobilized electrical charges comes in contact with an aqueous solution of mobile ions. For solid-liquid interfacial interactions, the consequent forces can be typically characterized in terms of the electrostatic potential that can fundamentally be quantified by the average potential in the surface of shear or what is often referred to as the streaming zeta potential ζ [52]. Thus, the electrokinetics and physisorption of ionic surfactants at the solid-liquid interface alters the surface wettability behavior considerably, and this can be correlated by the ionic exchange in the EDL that is directly reflected in the change in ζ.

As indicated earlier, the surface wettability of colloidal systems, which is a manifestation of molecular interactions between the liquid and solid in direct contact at the interface, can be represented by the liquid-solid contact angle [54]. In correlating it by the change in zeta potential ζ (which is an electrokinetic control parameter for the stability of hydrophobic colloids), distinct regions of change in adsorption and corresponding wetting variations are seen that are associated with the aggregation mode of adsorbed ions at the solid-water interface. This is evident in Fig. 10, for example, where the variation in zeta potential and measured contact angle with concentration in aqueous SDS (anionic) and CTAB (cationic) solutions are graphed. As seen from this graph, SDS displays a stronger adsorption than CTAB, which is reflected in the magnitude of zeta potential and the larger changes in contact angle. After the point of zeta potential reversal (PZR) [30, 52], also referred to as the isoelectric point (IEP), the slope of the ζ curve becomes negative for the anionic SDS and positive for the cationic CTAB because of the opposite charges they carry. This suggests that some adsorption may take place in reverse

orientation to form reverse hemimicelles [30], to render the surface increasingly hydrophilic. A bilayer is formed near CMC, and the contact angle tends to be constant as the surface becomes highly hydrophilic.

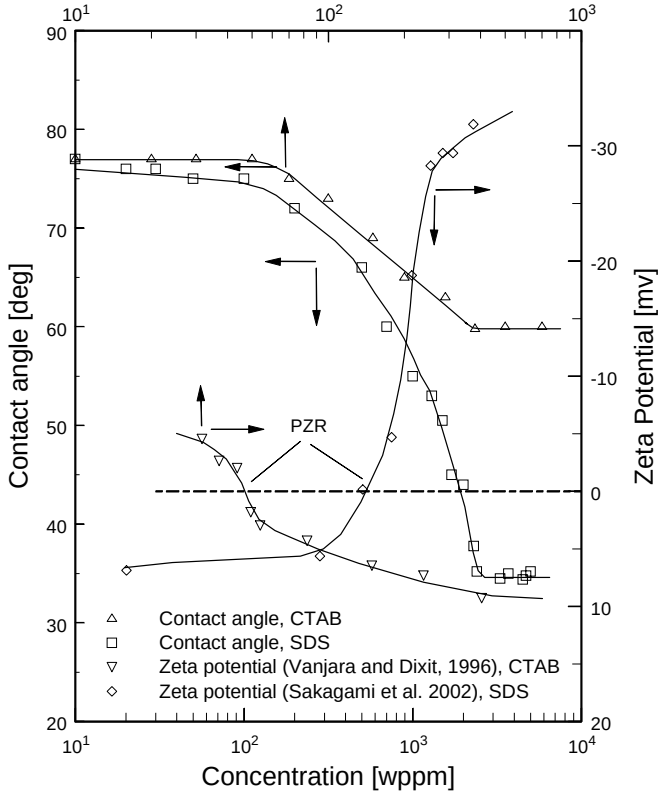

Figure 10. Correspondence between streaming zeta potential and liquid-solid contact angle in typical cationic CTAB and anionic SDS surfactant solutions [43].

Nucleate Boiling Heat Transfer

The altered pool boiling behavior over a cylindrical heater, where both enhanced heat transfer and suppressed boiling are seen, is represented by the variation in the relative heat transfer coefficient h in Fig. 11. Here data (relative to that of de-ionized distilled water) for aqueous solutions of three different surfactants (anionic SDS, cationic CTAB, and nonionic Triton X-305) are graphed [23-25, 55]. The heat transfer coefficient increases with concentration ($0 < C \leq$ CMC), and an optimum enhancement is seen in solutions at or near CMC,

or (C/C_{cmc}) = 1, where the additives are characterized by micelle formations [33]. But with C > CMC, the enhancement decreases and the heat transfer even deteriorates below that in pure water, particularly at low heat fluxes. Furthermore, as reported by Zhang and Manglik [43], there was early ONB (onset of nucleate boiling or bubble incipience) with $C \leq$ CMC, but delayed incipience when $C >$ CMC. In fact, a thermal hysteresis was seen in the latter case, which is characteristic of high wettability [56], and a much larger temperature overshoot was observed in SDS solutions with very high concentrations ($C \gg$ CMC) than that in corresponding Triton X-305 and CTAB solutions, and in that order. This performance correlates very well with the contact angle (or surface wetting) variations depicted in Fig. 8.

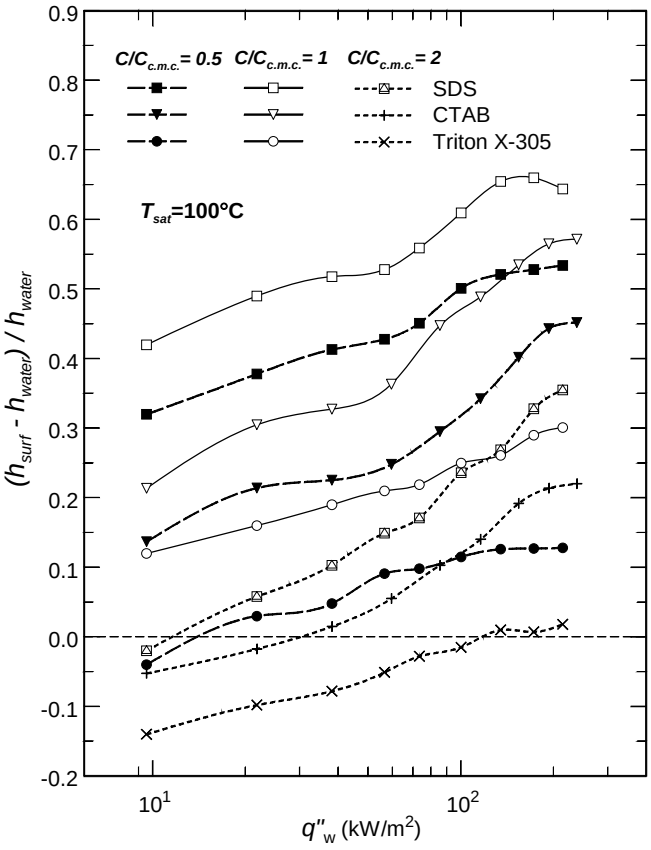

Figure 11. Boiling heat transfer performance of aqueous surfactant solutions.

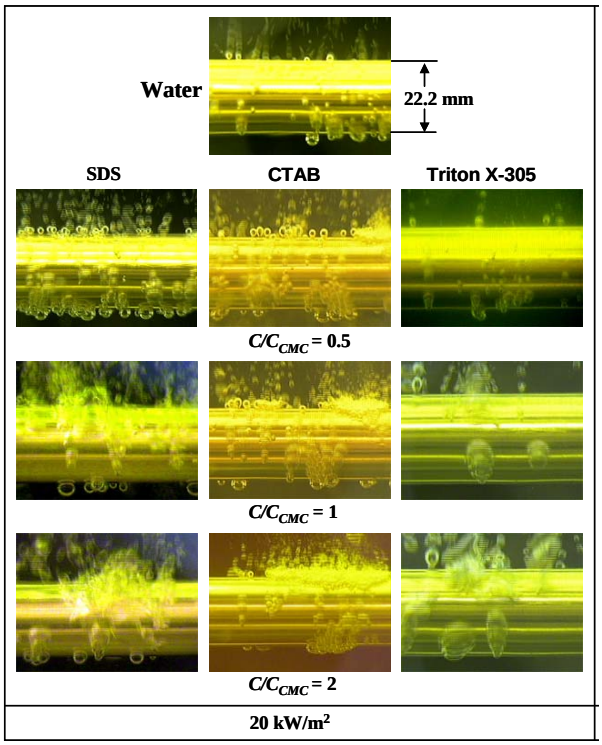

Figure 12. Ebullient signatures in saturated nucleate boiling of distilled water, aqueous SDS, CTAB, and Triton X-305 solutions.

That the primary boiling control is directly related to nucleation site activation and density (influenced by wetting) and bubble dynamics (growth through departure, influenced by interfacial tension) can be surmised from the photographic presentation of ebullience in Fig. 12. Compared to pure water, boiling in SDS and CTAB solutions is more vigorous with activation of smaller-sized, more regularly-shaped bubbles that nucleate in a cluster of sites. They have a significantly higher departure frequency, with virtually no coalescence of either the neighboring or sliding bubbles when $C < \text{CMC}$. However, when $C \geq \text{CMC}$, foaming patches begin to occur, the area of liquid-only-coverage on the heater surface increases, and slightly larger bubbles are formed. This is indicative of a change in surface wetting and it is more evident in the SDS solutions. Boiling with Triton X-305, on the other hand, shows much smaller-sized bubbles in pre-CMC solutions, and considerably fewer and larger-sized bubbles are formed with increasing

concentrations. This behavior contrasts from not only that of water but also of SDS and CTAB, and is predicative of the continuous increase in wetting (or decrease in contact angle θ; as seen in Fig. 8) with increasing concentration of this surfactant.

The observed ebullience in reagent-laden aqueous solutions and concomitant boiling heat transfer data cannot be explained simply by the reduced dynamic surface tension effects alone. If this were so, then the smallest-sized bubbles would be seen in C ≥ CMC solutions, where σ reaches the lowest possible value. Instead, because of the adsorption of surfactant molecules and their different orientations in the adsorption layer (Fig. 2), the heater surface has higher wetting with increasing concentration and larger nucleation cavities get flooded. Fewer bubbles are thus nucleated, and they tend to have relatively larger departure diameters, which is typical of ebullience in wetting liquids [9]. These variations in the bubble nucleation and its growth-departure dynamics, inter-relationship with reagent-induced wetting, and dynamic interfacial tension changes, clearly scale and correspond with the reagent's molecular dynamics (adsorption-physisorption and electrokinetics; schematically shown in Fig. 2).

The effects of heat flux and concentration on the nucleate boiling heat transfer in typical aqueous polymer (HEC-QP300) solutions are graphed in Fig. 13. A maximum enhancement of 22.9% in 600 wppm aqueous solution is obtained, and the improved performance tends to be rather weakly dependent upon the wall heat flux. Enhanced heat transfer in boiling of dilute (C < Cc.p.c. ~ 500 wppm) aqueous HEC-H solutions on a plate heater is also evident from the Kotchaphakdee and Williams [57] data. Furthermore, the decrease in boiling heat transfer enhancement in HEC solutions with $C > C_{cpc}$ (700 wppm, 1000 wppm, and 3000 wppm) is evident. In the 3000 wppm solution, up to 7.5% degradation in the heat transfer coefficient is seen for q''_w < 70 kW/m2 when compared to that in water; the degradation also tends to be

strongly dependent upon wall heat flux. On the other hand, a different polymer, Carbopol 934, and as seen in the ensuing, promotes no enhancement in heat transfer [21] and, in fact, there is significant deterioration in the boiling performance.

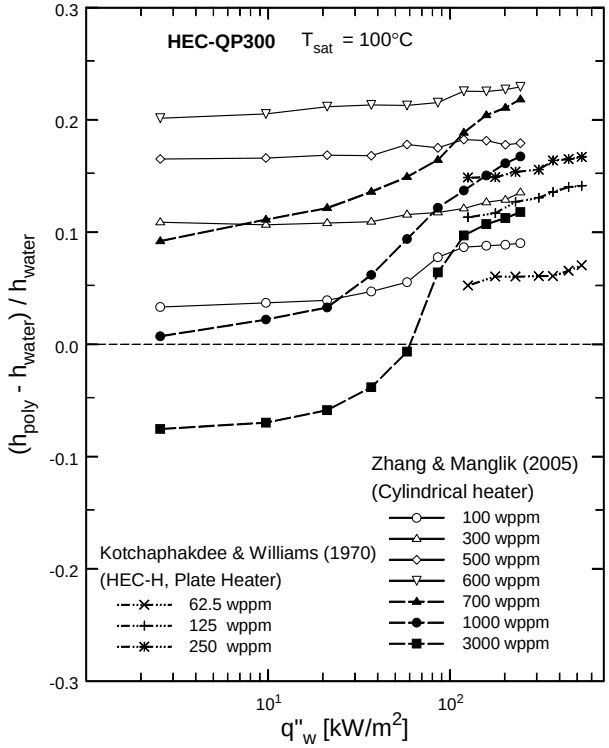

Figure 13. Variation of the relative boiling heat transfer coefficient of HEC-QP300 aqueous solutions with heat flux and polymer concentration [21].

The photographic records presented in Fig. 14 are typical of the nucleate boiling behavior of aqueous HEC-QP300 and Carbopol 934 solutions; a sample for deionized distilled water is provided for reference. The bubbling process in HEC solutions, distinct from that in Carbopol, is more vigorous, with smaller-sized and more regularly shaped bubbles that have a reduced tendency for coalescence when $C < C_{cpc}$. There is an early inception of bubbles with a faster covering of the heating surface and a higher bubble-departure frequency, which is essentially the outcome of reduced surface tension at the liquid-vapor interface. Also, molecular adsorption on

the heating surface may contribute to the formation of new sites [58], which in turn would explain the increase in number of bubbles as there was no change in the measured surface wettability [59]. However, at very large concentrations ($C > C_{cpc}$), the bubbles that originate at the underside of the cylindrical heater tend to coalesce and form bigger bubbles as they slide along the cylindrical periphery of the heater surface at departure. At the same time, there are some small patches that are covered by liquid, and no bubbles formed underneath these patches.

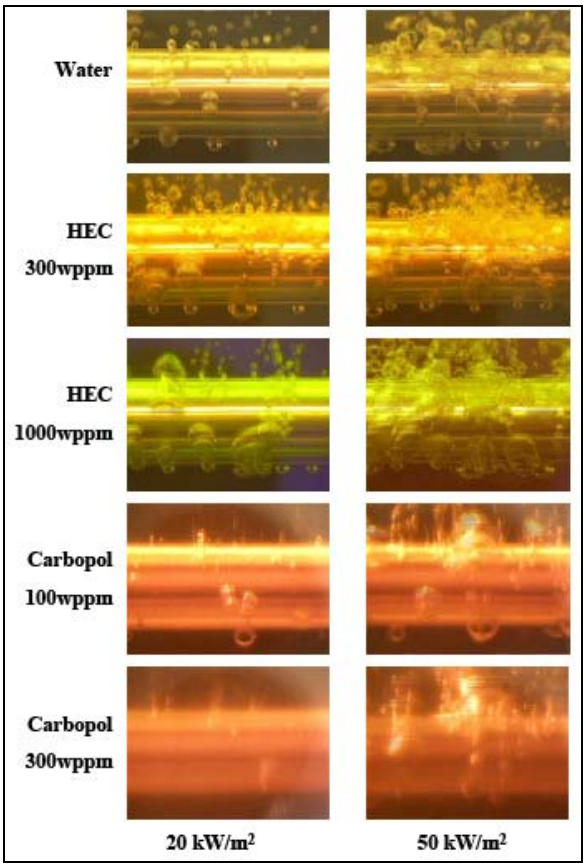

Figure 14. Ebullient behavior in nucleate boiling of water, and aqueous HEC-QP300 and Carbopol 934 solutions of different concentrations at different heat fluxes [21].

This behavior is quite contrary to that seen in boiling of surfactant solutions, in which foaming begins to occur or surface wetting condition significantly changes when $C >$ CMC [24, 25, 60]. Perhaps the significantly increased viscosity of higher concentration polymer solutions

tends to suppress the bubble nucleation process and growth of vapor bubbles. As a result, some nuclei do not get activated at all, and this also then leads to the deterioration of boiling performance in aqueous solutions with $C > C_{cpc}$. In the case of Carbopol 934 solutions, on the other hand, ebullience that is entirely different from that in water as well as HEC solutions is evident. There is considerable bubble suppression, along with dispersed vapor explosions (bright white spots captured in the picture; Fig. 14) in some regions of the heater surface. This kind of bubbling activity was also observed [61] in boiling of dilute polyethylene oxide (PEO) solutions. Moreover, there is delayed incipience, or ONB, and the sparsely formed bubbles have a slower departure frequency. This is essentially due to the increased viscosity of Carbopol 934 solutions, which lends to a higher drag resistance for the nucleating and departing bubbles to overcome.

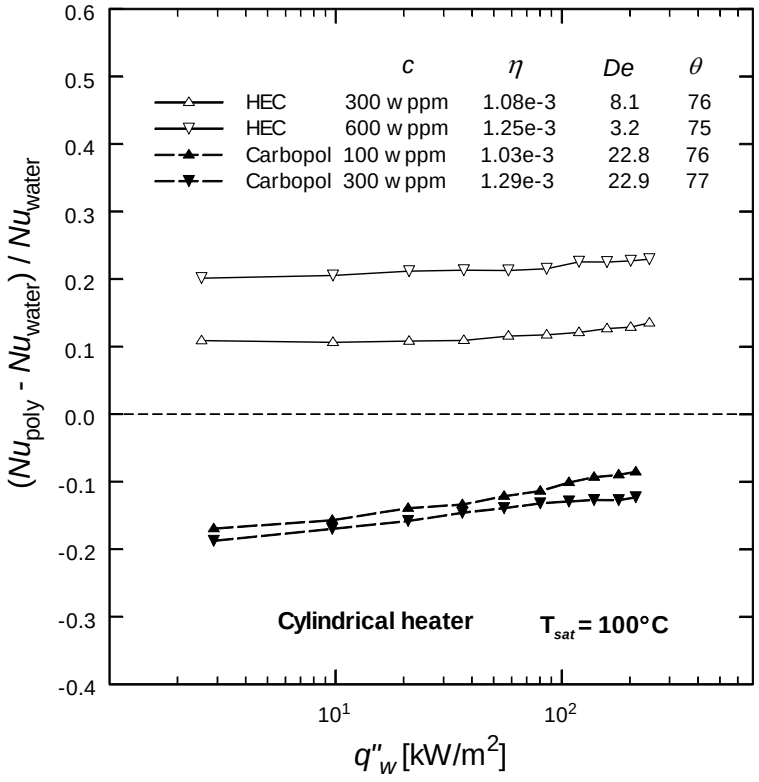

Figure 15. Effect of dynamic surface tension, represented by De, on the boiling heat transfer coefficient in aqueous polymer solutions [21].

In general, the reduction in dynamic surface tension (which decreases the required superheat for the onset of boiling), and the macromolecular adsorption on the heating surface (which could contribute to the formation of new nucleation sites and increased bubble frequency) are perhaps the two main factors for the enhancement of boiling heat transfer in low-concentration ($C < C_{cpc}$), surface-active HEC solutions. On the other hand, the decreases in the nucleate boiling heat transfer coefficients in HEC solutions with concentrations $C > C_{cpc}$), and pure shear-thinning Carbopol 934 solutions are possibly associated with the substantial increase in the liquid viscosity that tends to suppress micro-convection in the bubble boundary layer as well as retard the growth of vapor bubbles.

Finally, Fig. 15 provides further insights on the role of dynamic surface tension or surface-active effects on the heat transfer performance. While their respective concentrations are different, their apparent viscosities η are comparable, and heat transfer enhancement is seen in HEC solutions, whereas, contrastingly, there is only heat transfer deterioration in Carbopol solutions. The ability of a reagent to reduce surface tension under dynamic conditions can perhaps be characterized by a balance between the molecular diffusion time scale τ_d of the additive, and the typical time scale t of boiling in aqueous polymeric solutions. This can be generalized in terms of what could be considered as a modified Deborah number (Reiner, 1964) and defined as $\left(\mathrm{De} = \tau_d / t\right)$[1] to delineate the dynamic surface tension effect. It then follows that smaller values of De lend to more surface-active effects. This is seen from the data for 600 wppm HEC solution in Fig. 15, where De = 3.2 represents a much larger dynamic surface

[1] Contrary to expectations in the scientific literature, it is interesting to note that according to Wikipedia (URL: http://en.wikipedia.org/wiki/Deborah_number), the Israeli civil engineering professor Markus Reiner (1964) named this dimensionless time scale (ratio of a flow "relaxation time" and an "observed time") after a biblical prophetess Deborah. In most cases, however, dimensionless groups in fluid mechanics and heat transfer have been customarily named after the originators of the respective scaling, and are not coined on the basis of one's religiosity.

tension reduction compared to that in the larger De values of the other three solutions, and thereby a higher heat transfer performance. Considering that the only drastic physical property change in these four solutions is the dynamic surface tension relaxation, and that the surface wettability (or solid-liquid interface contact angle θ) for both HEC and Carbopol are close to that of water (77°), the results in Fig. 15 clearly suggest that the dynamic surface tension (inherent in Deborah number De) is perhaps one of the more significant predictive parameters.

Conclusions

Interfacial properties at the liquid-vapor (dynamic and equilibrium surface tensions) and solid-liquid (surface wetting or contact angle) interfaces characterize the adsorption behaviors of additives in their aqueous solutions. Surfactants lower the surface tension of water considerably, and their adsorption-desorption process at the liquid-vapor interface is time-dependent. This manifests in a dynamic surface tension behavior, which eventually reduces to an equilibrium value after a long time span. Also, the reagent physisorption process and electrokinetics tend to follow a characteristic adsorption isotherm at the solid-liquid interface, and the consequent changes in surface wetting or contact angle correlate well with the adsorption characterization or zeta potential.

Reflecting the altered interfacial properties, saturated nucleate pool boiling in aqueous surfactant solutions is altered significantly, with enhanced heat transfer in solutions with $C \leq$ CMC, which decreases and even deteriorates below that of pure water when $C >$ CMC. Besides the heat flux (or wall superheat) levels, the surfactant interfacial phenomena at both the liquid-vapor and solid-liquid interfaces govern the boiling bubble dynamics. The faster diffusion of lower molecular weight surfactants tends to reduce the surface tension faster in a short period of

time, which results in the better heat transfer performance of their solutions. Accordingly, because of the highly dynamic, small-surface-age-interface nature of the bubbling activity in nucleate boiling, the dynamic surface tension relaxation becomes a more effective scaling parameter rather that the equilibrium value. The altered wettability of heater surface due to the physisorption of surfactant molecules at the solid-liquid interface can be fundamentally decoupled from the change in gas-liquid interfacial tension, and thereby provides a critical mechanism for controlling (enhancing or suppressing) on demand the nucleate pool-boiling behavior of water-based solutions.

In aqueous polymer solutions, the boiling behavior is altered essentially due to the changes in rheological and interfacial characteristics. While they are generally more viscous than water, and can also exhibit a distinct shear-rate dependent non-Newtonian shear-thinning rheology, surface-active nature and molecular adsorption at the vapor-liquid interface in HEC-QP300 solutions shows greater relaxation of both dynamic and equilibrium surface tension in comparison with Carbopol 934. As a consequence, in HEC solutions with $C < C_{cpc}$ (or $C <$ the critical polymer or overlap concentration) there is considerable heat transfer enhancement, characterized by an ebullient signature that has larger number of smaller bubbles that have much higher departure frequencies than that in pure water. The reduced surface tension, along with the molecular adsorption on the heating surface (liquid-solid interface) perhaps also contributes to the formation of new nuclei, and smaller Deborah number De lends to higher surface-active effects. In post-C_{cpc} solutions, however, there is a decrease in the heat transfer coefficient from the maximum value obtained at C_{cpc}. This is perhaps due to the retardation of vapor bubble growth and suppression of micro-convection in the boundary layer because of the high viscosity of high concentration solutions. Some vapor explosions are also observed on the heater surface

in Carbopol solutions, akin to the boiling behavior normally found in highly viscous liquids. Finally, the results suggest that the dynamic surface tension (as in the case of surfactants) and apparent viscosity are the primary performance predictors, and their "designed" variations can lend to the control of nucleate boiling heat transfer in aqueous solutions.

Nomenclature

C concentration [wppm]

C_{cmc} critical micelle concentration or CMC [wppm]

C_{cpc} critical polymer/overlap concentration or CPC [wppm]

g gravitational acceleration [m/s^2]

h boiling heat transfer coefficient [W/m^{2}K]

q''_w heater wall heat flux [W/m^2]

t time or time scale [s]

η apparent viscosity of a polymeric solution

θ contact angle [°]

θ_a advancing contact angle [°]

σ surface or gas-liquid-interfacial tension [N/m] or [mN/m]

τ surface age and/or time [s]

τ_d diffusion time scale [s]

τ_g bubble growth time [s]

τ_w waiting time for a nucleating bubble [s]

ζ streaming zeta potential [mV]

NUCLEATE POOL BOILING IN AQUEOUS POLYMERIC SOLUTIONS

Introduction

The ability to enhance and perhaps even control boiling, given its high heat removal efficiency, presents an exceptional thermal management opportunity for a broad spectrum of new and emerging applications [62, 63]. An attractive method of altering nucleate pool boiling in water systems is to add reagents and/or polymers in controlled concentrations [6, 21, 23, 25]. The associated heat transfer and phase-change bubble dynamics are governed by a complex interplay of interfacial behavior (vapor-liquid interfacial tension and liquid-solid surface wetting), and rheological properties of the solution. Reagents or surfactants primarily alter the surface tension and wetting of the solvent. Certain types of polymers, on the other hand, besides being surface active also render the solution a non-Newtonian viscous property.

There has been growing interest in the literature in using polymers in semi-dilute aqueous solutions to enhance or alter nucleate boiling heat transfer, as pointed out in a recent review [21]. The reported results span a wide spectrum of phase-change characteristics, which are sometimes contradictory. For instance, Kotchaphakdee and Williams [57] found the boiling heat transfer from a plate heater to be enhanced in shear-thinning HEC-H and PA-30 solutions, of which HEC-H also reduces surface tension. Contrarily, in experiments with platinum wire heaters, Wang and Hartnett [64], and Paul and Abdel-Khalik [65], a deterioration in heat transfer was found in very dilute aqueous polymeric solutions when compared to that in water. To complete the quorum of dissimilar results, Yang and Maa [66] report that the boiling heat transfer performance for dilute aqueous HEC solutions is independent of heater shape (plate or platinum wire). The data of Shul'man et al. [67], and Levitsky et al. [58] with a plate heater and HEC-H

solutions in water indicate enhanced boiling heat transfer in dilute solutions ($C = 0.015\times10^{-9}$ to 0.5×10^{-9} mol/cc), but decreased heat transfer in higher concentrations ($C = 10\times10^{-9}$ mol/cc).

The addition of some polymers in water primarily alters the solution rheology, which increases with concentration and also has a shear dependent viscous behavior [38, 68]. However, depending upon their molecular chains, such polymers may also have surface-active properties, and hydroxyethyl cellulose (HEC) and polyethylene oxides (PEO) are good examples [21, 35, 40]. In such cases, due to their molecular adsorption at the vapor-liquid and liquid-solid interface, there is some relaxation of the interfacial tension and increase in wetting of the solution [21, 33], which varies with polymer chemistry and its concentration. This significantly changes the ebullient behavior, or the bubble nucleation and departure dynamics, during boiling when compared to that in pure water [21, 58]. Higher surface wetting delays incipience [7, 9] but interfacial tension relaxation tends to aid smaller bubble departure and enhanced heat transfer [6, 25]. The increased viscosity of the solutions, on the other hand, tends to counter this and has an adverse impact on boiling heat transfer [21, 65]. The bubble growth rate and departure frequency tends to get impaired due to higher viscous drag, especially in the incipience and partial boiling regime [21]. Nevertheless, it may be hypothesized that the shear-thinning character of some polymeric solutions would tend to mitigate this effect during higher heat flux boiling of the fully-developed regime, where higher shear rates are exerted at bubble interfaces due to their substantially higher departure frequencies. This suggests a multifarious inter-relationship, which could range from countervailing to collaborative effects of the non-Newtonian viscous behavior, surface wetting, and dynamic interfacial tension relaxation.

The objective of the present study is to parametrically explore the effects of shear-dependent viscosity, along with those due to the changes in dynamic vapor-liquid interfacial tension and

liquid-solid surface wettability of aqueous solutions of a surface-active polymer on their nucleate pool boiling heat transfer performance. A nonionic soluble polymer, hydroxyethyl cellulose (HEC) and its grade QP-300 (molecular mass ~ 600 kg/mol), is used as the control additive in deionized distilled water solutions. The rheological and interfacial properties of the HEC QP-300 solutions in different concentrations are recorded, which exhibit viscous shear-thinning, dynamic surface tension relaxation, and increased wetting (reduced contact angle) behaviors. Saturated pool boiling heat transfer at atmospheric pressure is measured in a controlled set of experiments with an electrically heated, horizontal cylindrical heater by mapping the variation of the applied wall heat flux q''_w with wall superheat ΔT_{sat}. The presented results characterize ebullient phase-change heat transfer from incipience or ONB to the fully developed nucleate boiling regime, and highlight the effects due to the pseudoplasticity, dynamic interfacial tension relaxation, and altered wettability of the aqueous solutions at different polymer concentrations. Furthermore, the associated bubble generation activity is photographically recorded to provide additional mechanistic insights to the vapor generation process.

Experimental Method and Materials

Polymer solutions

The grade QP-300 of hydroxyethyl cellulose (HEC), a nonionic cellulose polymer, which is used in this study, has an idealized molecular structure shown in Fig. 1. It has a molecular mass of ~ 600 kg/mol, and it not only renders aqueous solutions with a non-Newtonian pseudoplastic (or shear thinning) rheology but also exhibits properties of a surface-active reagent (reduces surface tension). The required aqueous solutions for the experiments were prepared by adding precise quantities of HEC QP-300 powder, measured using an electronic weighing scale with

±0.01 g accuracy, to deionized distilled water in a beaker. The homogeneity of the solution was assured by stirring it sufficiently on a magnetic stirrer so as to keep the mass moving continuously. To achieve this, approximately four hours of gentle stirring was required for complete hydration of HEC powder, and the solution was then allowed to age overnight by continuing to stir it at very slow speeds.

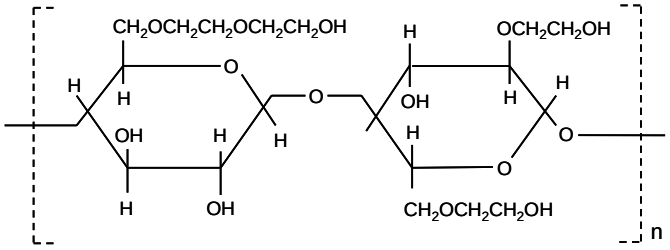

Figure 1. Schematic representation of the idealized molecular structure of the polymer hydroxyl ethyl cellulose (HEC QP-300).

Pool boiling experiment

Figure 2(a) provides the schematic (not to scale) of the apparatus used in this study for conducting nucleate pool boiling experiments. It consists of two large corning glass vessels, where the inner glass tank, which holds the polymer solution and the cylindrical heater, is incased in the outer glass tank. Silicon oil (50 cSt), fed from a constant-temperature re-circulating bath (not shown in the figure), is circulated in the outer vessel in order to maintain the test pool at its saturation temperature. To ensure this, the oil was maintained at a temperature (~ 135°C) greater than the saturation temperature of the test fluid, so as to form a thermal jacket around the pool; NESLAB's RTE-221 oil bath circulator was used for heating and circulating the silicon oil. An auxiliary electrical cartridge heater, immersed in the pool, was used to heat up the pool quickly to its saturation temperature (using the oil bath alone takes much longer time). A water-cooled reflux condenser, along with an additional coiled-tube water-cooled condenser,

were used to condense the generated vapor and maintain an atmospheric-pressure, constant level pool. A U-tube manometer is mounted on top of the inner vessel, and it monitors the pool pressure with a 0.001 atm (5 mm of water column) visual accuracy throughout the pool boiling experiments.

The heating test section (described in Fig. 2b) consists of a horizontal, gold plated, hollow copper cylinder of 22.2 mm outer diameter that encapsulates a 240 V, 1500 W cartridge heater, which has insulated and sealed (to prevent any water encroachment short-circuit) lead wires. The 0.0127-mm thick gold plating on the copper sleeve mitigates surface degradation and oxidation from the test fluids. The heater is press-fitted inside the hollow cylinder with conductive grease so as to provide good heat transfer contact with the inner walls of the outer sleeve, and the end gaps on either side are filled with silicone rubber to prevent direct water contact. Extended details of the heater test section construction and its surface characterization, which has surface roughness ranging from r.m.s. values of 0.076 μm to 0.347 μm, as measured by an atomic force microscope, are given elsewhere [23, 69].

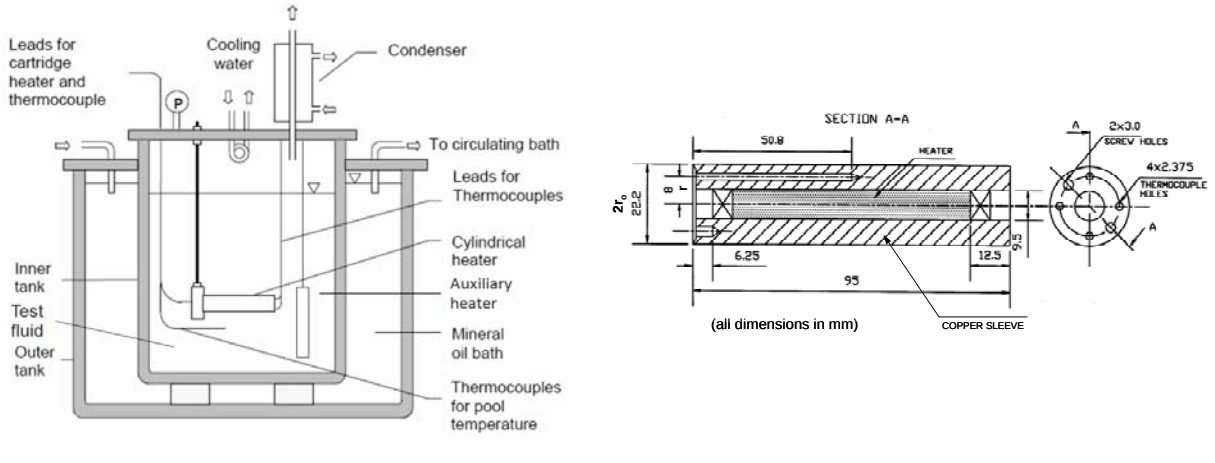

Figure 2. Experimental apparatus: (a) schematic of pool boiling set up, and (b) constructional details of cylindrical heater assembly.

The heater-wall and pool-bulk temperature measurements were made with precision (±0.5°C) copper-constantan thermocouples, connected to a computerized data acquisition system with an in-built ice junction and calibration curve. A variac-controlled AC power supply, a current shunt (0.15 Ω with 1% accuracy), and two high-precision digital multimeters for current (±2.5% accuracy) and voltage (±1.5% accuracy) were used to record the input electric power and thus determine the heat load. At each incremental value of power input or heat load, the dissipated wall heat flux q''_w was computed from the measured voltage *V*, current *I*, and heater surface area *A* (= $2\pi r_o L$; where *L* is the length of heated heater) as,

$$q''_w = (VI/A) \tag{1}$$

In these calculations, the actual voltage drop across the heater and the actual current flowing through it (measured directly across the precision shunt resistance in series with the heater) were recorded directly to provide the actual heat load, which inherently calibrates for any temperature-dependent variations in resistance [70, 71]. The wall superheat ΔT_{sat} for this heat flux was determined from the heater-wall temperature T_w, taken as the average value of four wall-temperature thermocouples reading ($T_{i,r}$) that are embedded in the heater surface, and the saturation temperature T_{sat} of the liquid pool as follows:

$$T_w = \left[\frac{1}{4} \sum_{i=1}^{4} \left\{ T_{i,r} - \left(q''_w r_o / k \right) \ln \left(r_o / r \right) \right\} \right] \tag{2}$$

$$\Delta T_{sat} = \left(T_w - T_{sat} \right) \tag{3}$$

where *r* is the radius of wall thermocouple location, r_o is the cylinder heater radius, and *k* is the thermal conductivity of heater material. The maximum experimental uncertainties were calculated by the single-sample propagation of error method [72] were ±2.92% and ±0.33%, respectively, for q''_w and ΔT_{sat}.

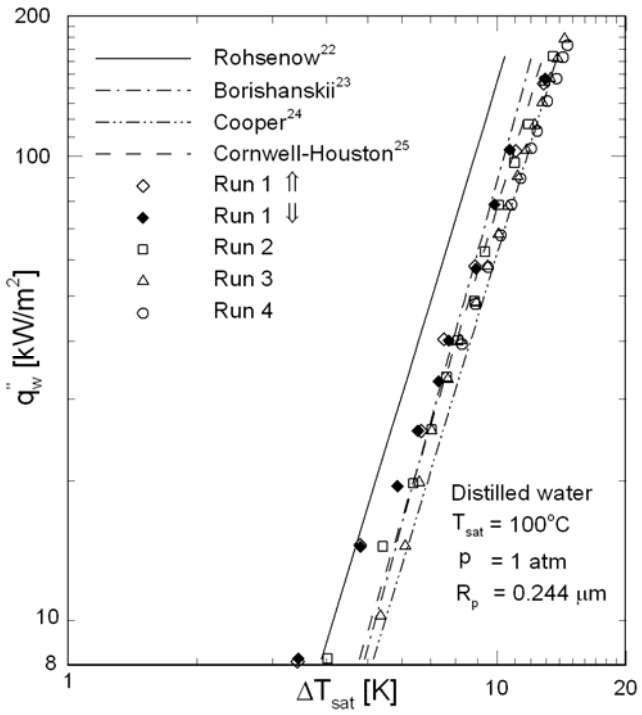

Figure 3. Nucleate pool boiling data for de-ionized distilled water and comparison with predictions of several correlations (Note: ⇑ and ⇓ indicates, respectively, data for increasing and decreasing wall heat flux).

Before the start of any experimental measurements, the pool was thoroughly degassed by first heating it to the saturation temperature by using the auxiliary heater, and then boiling it at a low heat flux while constantly maintaining it at T_{sat}. Power to the auxiliary heater was then cut off and the system was allowed to attain stable, saturation conditions; this entire process took about two-to-three hours to complete [69]. For the first set of experimental measurements, nucleate pool boiling with distilled, de-ionized water was recorded, with multiple runs over a period of six months so as to establish repeatability and the effects of aging of the heater surface. These results [69] are presented in Fig. 3, where the pure water boiling data are seen to be in good agreement with some previous data [23, 25], and are also within the envelope of predictions given by the much cited Rohsenow [73], Borishanskii [74], Cooper [75], and Cornwell-Houston [76] correlations. These data and the comparisons provide not only the

necessary validation of measurements and data acquisition methods, but also form the essential baseline water results for evaluating and contrasting the boiling performance of aqueous polymeric solutions.

Photographic record of boiling

A PULNiX TMC-7 series high-speed CCD camera was used to capture the visual dynamics of bubble generation, growth, and motion during boiling. It has a digital resolution of 768(horizontal) × 494(vertical) pixels, with eight different shutter speeds that go up to 1/10,000 sec. The camera is also fitted with FUJI 12.5 mm × 75 mm zoom lens for capturing close-up photographs during different stages of boiling. The camera was interfaced with a PC using a USB-based digital image capture and processing system (DQP-A4 Premier), which records consecutive frames of video in real-time images at 60 frames/s.

Viscosity measurement

Viscosity measurements were made using a rotating cup-and-cylinder rheometer (AR-2000, TA Instruments, Inc.) and a set of five Cannon-Fenske capillary-tube viscometers of different capillary diameters. The test solution were prepared by carefully adding a precisely weighed (±0.1 mg accuracy on an electronic scale) quantity of polymer powder to de-ionized distilled water. The mixture was then stirred at a constant speed on a magnetic stirrer till the powder dissolved completely, and the solution was then aged over a period of 10-12 hours before making viscosity measurement. Using the concentric cylinder assembly in the AR-2000 rheometer, apparent viscosity data in the shear-rates range of 10 s^{-1} to 400 s^{-1} were obtained, where the temperature control was maintained by the built-in Peltier heating system in the rheometer. The

higher shear rate data were obtained from the set of capillary-tube viscometers; note that the shear rate in these instruments is a function of their respective capillary diameters. Furthermore, a capillary-tube viscometer was also used for the measurements with weak concentration aqueous solutions so as to obtain the intrinsic viscosity, or the limiting viscosity number of the polymer [33, 77, 78]. Once again, the maximum single-sample error propagation method based uncertainty [72] in viscosity and temperature were ±1.4% and ±0.5%, respectively.

Surface tension measurement

Both the equilibrium and dynamic surface tension, or the gas-liquid interfacial tension, measurements of the polymer solutions were made using a tensiometer (SensaDyne QC6000; Chem-Dyne Research Corp.) that operates on the maximum bubble pressure method. It has two glass capillary-tube orifices of unequal diameters that are immersed in the test fluid pool in a beaker. The test fluid is maintained at a constant temperature, which is measured using a well-calibrated thermistor (±0.1°C precision) attached to the orifice probes. When dry air is bubbled through the orifices, a differential pressure signal is produced, which is proportional to the gas-liquid interfacial tension. Also, the time interval between the newly formed interface and the point of bubble break-off at the orifice mouth is referred to as the *surface age* τ of interface. It gives the measurement of bubble growth time that corresponds to the dynamic surface tension value at a given operating bubble frequency. Thus, by altering the air-bubble frequencies through the probes, both equilibrium and dynamic surface tension can be measured; the equilibrium data are obtained with very low bubble frequencies that lead to static or unchanging conditions. Extended details of the calibration techniques, data-acquisition methods, and measurement validation procedures are given in [35]. Furthermore, the maximum uncertainties,

ascertained from a single-sample error-propagation method [72], in the measured solution concentration, temperature, and surface tension were found to be ±0.4%, ±0.5%, and ±0.7%, respectively.

Contact angle measurement

The static contact angle was measured with a sessile-drop goniometer. A small drop of the test solution was carefully deposited on a stainless steel specimen substrate that was placed under the goniometer lens. A precision micro-syringe was used to produce a droplet of desired liquid volume (~ 2-3 μl; drop volume ≤ volume of a spherical drop with a radius equal to the capillary length[2] l_c), which was carefully placed on the specimen substrate. The contact angle was measured for several new droplets placed at different surface locations on the substrate after allowing a one-minute settling time in each case. The goniometer radius line was aligned tangentially to the edge of the droplet touching the substrate specimen, and the contact angle was then directly measured from the angular scale engraved on the eyepiece. The minimum precision in this measurement was ±0.5°.

Results and Discussion

Aqueous solutions of hydroxyl ethyl cellulose (HEC) QP-300, except in low concentrations, generally display a viscous pseudoplastic behavior. This non-Newtonian characteristic is pointed out by Fig. 4, where the variations in shear-rate dependent apparent viscosity (η = shear stress / shear rate) are graphed for HEC QP-300 solutions in there different concentrations. At low shear

[2] This is the characteristic length scale for a liquid droplet that represents the balance between gravitational and surface tension forces. Thus, a sessile drop volume with an equivalent spherical radius less than l_c would have negligible influence of its weight and its spread on any substrate would be dominated by surface tension and consequent wetting alone.

rates the solution rheology tends to be Newtonian, with a significantly higher viscosity than the solvent, and the shear-thinning non-Newtonian flow manifests only at high shear rates. The consequent apparent viscosity behavior can be represented by the modified cross model [79-81]. This constitutive relationship, for the case of a negligible infinite shear-rate asymptote, in essence, is functionally the same as the modified power-law model [82], and can be expressed as

$$\eta = \eta_o \left[1 + \left(\eta_o / K \right) \dot{\gamma}^{1-n} \right]^{-1} \tag{4}$$

For the rheology of three HEC QP-300 solutions graphed in Fig. 4, the range of the characteristic parameters are $1.35\times10^{-3} \le \eta_o$ [N·s/m^2] $\le 3.25\times10^{-3}$, $0.42 \le K$ [N·s^n/m^2] ≤ 7.45, and $0.12 \le n \le 0.6$. The low values of flow-behavior index n are indicative of the highly shear-thinning or pseudoplastic property of these solutions.

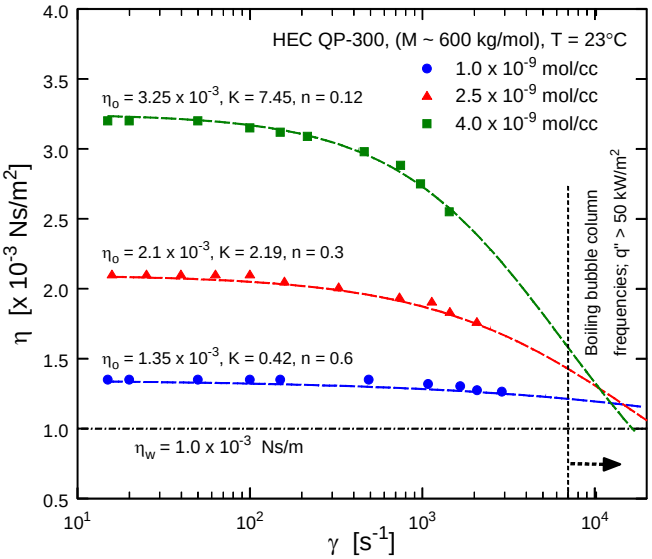

Figure 4. Shear-rate dependent apparent viscosity variation for different concentrations of aqueous HEC QP-300 solutions.

A more fundamental measure of the ability of a polymer to alter the solvent viscosity in solution, is the intrinsic viscosity [η] of the polymer [78, 83]. Also referred to as the limiting

viscosity number, and as Staudinger's index in older literature [84], the intrinsic viscosity $[\eta]$ for HEC QP-300 was determined by measuring the viscosity η with several different weak-concentration aqueous solutions using a capillary viscometer. From these measurements and knowing the solvent viscosity η_s (water in this case), the specific viscosity η_{sp} and relative viscosity η_{rel}, respectively, for each dilute concentration solution can be determined as follows:

$$\eta_{sp} = \left[\left(\eta - \eta_s \right) / \eta_s \right], \text{ and } \eta_{rel} = \left(\eta / \eta_s \right)$$

Thus, by extrapolating the graph of $\left(\eta_{sp} / C \right)$ versus C to zero concentration, the intercept of the consequent Huggins plot gives the value for $[\eta]$; this can also be obtained from the intercept of the Kraemer plot through the graph of $\ln\left[\eta_{rel} / C \right]$ versus C. The two plots are given in Fig. 5, and the average value of $[\eta]$ for HEC QP-300 was determined to be 5.29 dl/g. This limiting value at infinite dilution is a direct measure of the molecular properties of the polymer, and it essentially quantifies the volume occupied by a unit mass of the macromolecule. Higher $[\eta]$ suggests increased capability of a polymer to enhance the solution viscosity, and in general it is related to the molecular weight or degree of polymerization [77, 85, 86].

The variation in equilibrium surface tension, or the liquid-vapor interfacial tension, with different bulk concentrations of the polymer HEC QP-300 in water is graphed in Fig. 6. The surface tension is seen to continually decrease from that of the solvent (water; σ_w = 72.4×10^{-3} N/m) to a minimum asymptotic value of 66.8×10^{-3} N/m. The concentration that demarcates the lower inflection point in the $\sigma - C$ isotherm, i.e., the point of transition to the minimum surface tension asymptote, often coincides with the critical polymer concentration (cpc) or overlap concentration C^* [21, 85, 87, 88]. At cpc or C^*, polymer agglomeration or coil entanglements begin to form in solution, which would then be in the semi-dilute regime. This interfacial

tension relaxation is a diffusion-rate dependent behavior, which is generally governed by the bulk concentration and diffusion-adsorption kinetics of the polymer-solvent systems [50]. The critical polymer concentration, as discerned from Fig. 6, is estimated to be ~ 1.0×10^{-9} mol/cc (~ 600 wppm).

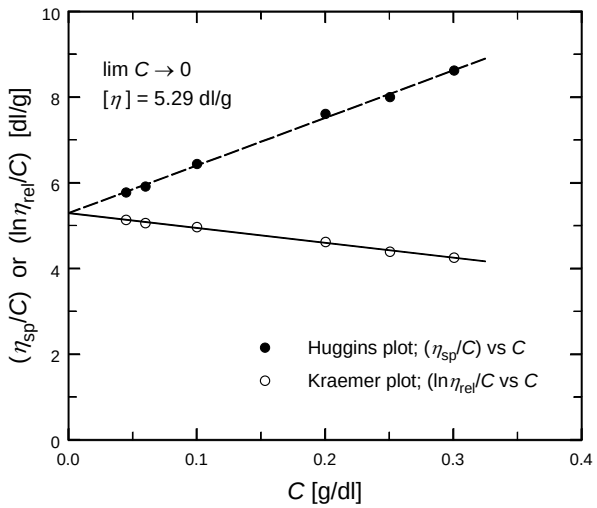

Figure 5. Intrinsic viscosity $[\eta]$ of HEC QP-300.

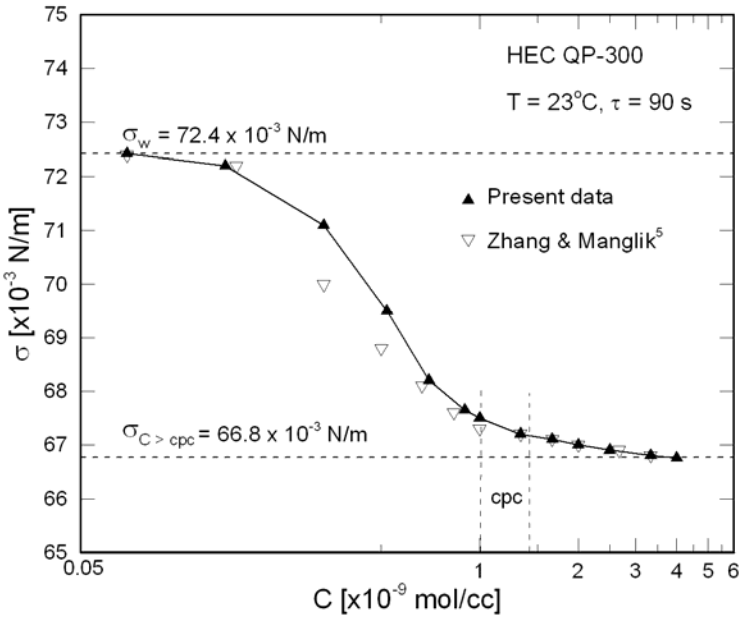

Figure 6. Equilibrium gas-liquid interfacial tension (surface tension) and its variation with polymer concentration in aqueous solution.

The critical overlap concentration can also be determined from the intrinsic viscosity [77, 83, 85, 86], because $[\eta]^{-1}$ approximately represents the concentration within the polymer, or its overlap concentration in a solvent, exceeding which molecules will touch and interpenetrate to form a semi-dilute solution. According to the Einstein model, which considers dilute dispersions of unsolvated spherical particles, when the volume fraction ϕ of the spherical particles is small the relative viscosity is given by the following function [83]:

$$\frac{\eta}{\eta_s} = 1 + 2.5\phi + k_1\phi^2 + \ldots \tag{5}$$

From the limiting condition of Eq. (5) it can be shown [83, 86] that as $\phi \to 0$ the overlap concentration can be approximated as $C^* \approx 0.25[\eta]^{-1}$. Thus, from the intrinsic viscosity given by the plots in Fig. 5, the critical polymer concentration is obtained as $C^* \approx 0.79\times10^{-9}$ mol/cc. This value is the same order of magnitude as that obtained from the gas-liquid interfacial tension adsorption isotherm of Fig. 6, and corroborates the latter results.

Furthermore, that the liquid-vapor interfacial tension relaxation is a time-dependent process is demonstrated by the σ versus τ plots of Fig. 7. Here, the change in surface tension σ with surface age τ, or the time period of a newly formed bubble from inception to departure, is graphed for aqueous solutions of HEC QP-300 with bulk concentrations of $1.0\times10^{-9} \le C \le 4.0\times10^{-9}$ mol/cc. It is seen that a finite time is required for complete interface relaxation, or to attain an equilibrium between the surface and bulk concentrations. Generally a surface age of $\tau > 1.0$ s is needed for this condition, and for $\tau < 50$ ms, the interfacial tension essentially corresponds to that of the solvent (water); the interim period of 50 ms $< \tau <$ 1.0 s is characterized by sharp gradients in σ. It may be noted here that the values for σ at very small surface age are extrapolated from the time-dependent adsorption isotherm fit through the data by the method

outlined by Hua and Rosen [89]. Also, there is little difference between the data for 2.5×10^{-9} and 4.0×10^{-9} mol/cc solutions, suggesting micelle agglomeration or coil entanglements of the polymer at these concentrations. This dynamic surface tension behavior, which is facilitated and governed by the molecular mobility of the polymer in solution and its interfacial adsorption [35, 42, 50, 89] at an evolving gas-liquid interface, lends to the modification of ebullience that characterizes the attendant boiling heat transfer.

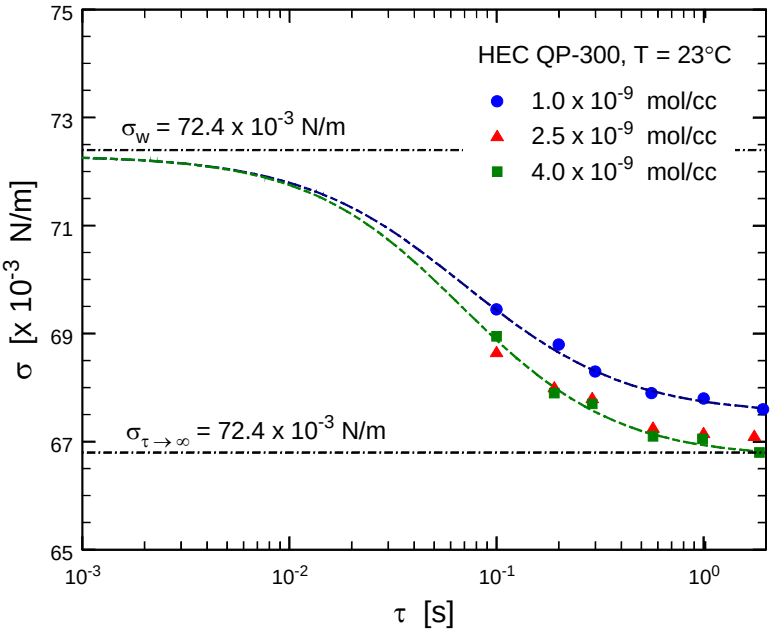

Figure 7. Temporal variation of dynamic surface (gas-liquid interfacial) tension for different polymer concentration aqueous solutions.

The change in wetting, manifest at a liquid-solid interface, can be ascertained by the contact angle θ, and its variation with concentration C of HEC QP-300 in aqueous solutions is graphed in Fig. 8. The measurement is for a metallic substrate (stainless steel), and θ is seen to decrease with increasing C till a lower constant-value asymptote is attained. The minimum contact angle plateau is further seen to be attained when $C > C^*$ (the overlap concentration), where molecular

agglomeration of the polymer begins to form in solution. This is representative of typical physisorption behavior of surface-active solutes at liquid-solid interfaces, and where wetting is influenced by the kinetics of interfacial molecular adsorption [54, 90].

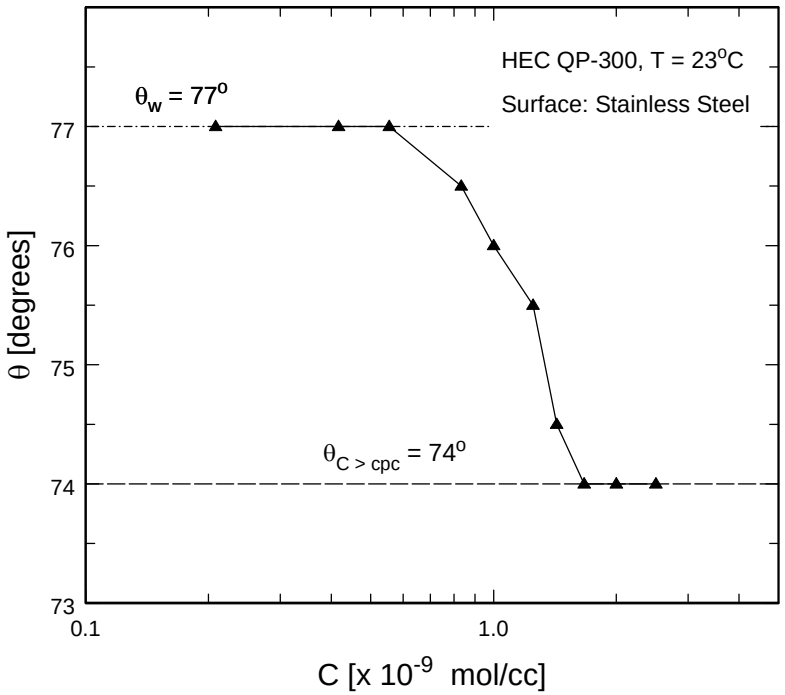

Figure 8. Change in contact angle with concentration of aqueous HEC QP-300 solutions.

In general, the boiling behavior of a liquid is altered by the changes in its surface tension, rheology, and heater surface wettability. While wetting of the heater surface controls nucleation and the site density thereof, gas-liquid interfacial tension and shear-dependent viscosity of a polymeric solution alters the post-nucleated bubble dynamics [6, 21, 25]. The pool boiling curves presented in Fig. 9 for different concentrations of aqueous HEC QP-300 solutions, along with that for distilled and deionized water, quantify this ebullient heat transfer behavior. The substantial leftward shift in the $q''_w \sim \Delta T_{sat}$ curve for $C = 1.0\times10^{-9}$ mol/cc (~ C* or cpc) relative to that for water is indicative of the heat transfer enhancement over the entire range of heat flux

considered in the experiments. This specific case represents the largest overall enhancement, which is consistent with the previous finding that the highest boiling performance is attained with critical or overlap concentration of the polymer [21]. However, an anomalous boiling behavior is seen in solutions with higher concentration (C = 2.5×10^{-9} and 4.0×10^{-9} mol/cc). There is a significant rightward shift in the boiling curve where the heat transfer is even less than that in water in the low-heat-flux partial-boiling regime, followed by much larger enhancement, relative to that with C*, at higher hear fluxes (> 100 kW/m^2) or the fully-developed boiling regime.

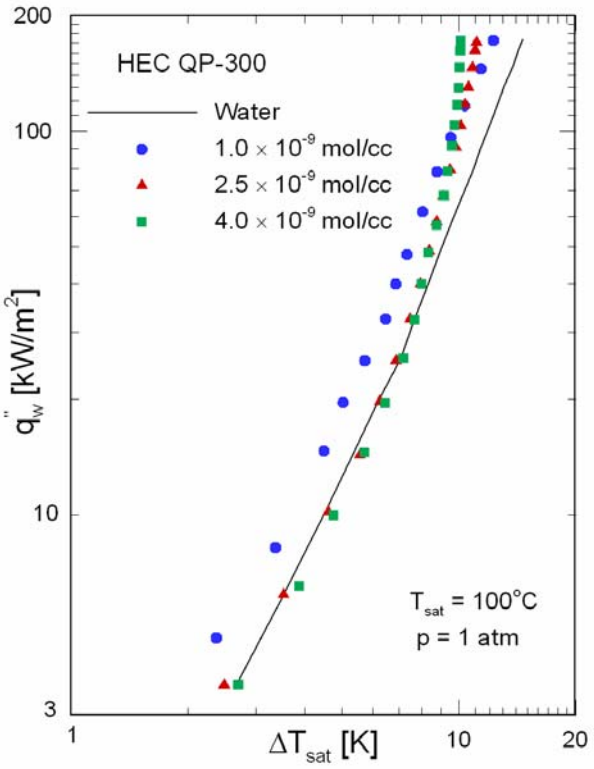

Figure 9. Nucleate pool boiling data for different concentrations of aqueous HEC QP-300 solutions, along with that for distilled, de-ionized water.

A much clearer and quantitatively amplified delineation of the boiling performance of the three different concentration solutions of HEC QP-300, relative to that in distilled water, is

presented in Fig. 10. The variation of the enhanced heat transfer coefficient, quantified by the dimensionless ratio $\left[\left(h-h_w\right)/h_w\right]$ with the heater-wall heat flux q''_w is graphed. The consistent and virtually constant enhancement of about 20% in the 1.0×10^{-9} mol/cc (~ C^*) HEC concentration aqueous solution is evident in Fig. 10, along with the agreement with previous data [21]. As indicated earlier, the more curiously unexpected set of results are those for solutions with $C = 2.5\times10^{-9}$ and 4.0×10^{-9} mol/cc. In these cases, there is a reduction (or degradation with respect to pure water) in heat transfer when q''_w < 30 kW/m^2, but much larger enhancement than that with C^* when q''_w > 100 kW/m^2. The higher of the two concentrations lends to about 6% decrease in heat transfer when compared with water for 7 < q''_w < 30 kW/m^2. This is a direct consequence of the higher polymeric solution viscosity (2-to-3× water, as seen in Fig. 4) at low shear rates and the consequent drag effects at the liquid-vapor interface of ebullient transport in the partial boiling regime. With increasing heat flux and hence larger vapor generation, the interfacial shear rate increases and thereby the viscosity of the shear-thinning solutions decreases; at very high shear rates the higher concentration solution even becomes less viscous than the lower C ones (see Fig. 4). As a result, the retarding viscous forces at the bubble-liquid pool interface become less significant and the low-surface-tension-driven enhancement, characterized by smaller and higher frequency bubble generation, is re-established with peak heat transfer performance attained when q''_w > 100 kW/m^2.

The nucleate boiling performance can further be characterized by the respective ebullient signatures in the three solutions at different heat fluxes. Photographic records of the vapor production that characterize the boiling history for increasing heat flux (q''_w = 20, 40 and 115 kW/m^2) are presented in Fig. 11. The bubble generation features, described by their relative

shape, size, coalescence activity, and surface density and distribution in the polymer solutions are seen to be very distinct from that in water. The boiling is more vigorous in $C \sim C^*$ (= 1.0×10^{-9} mol/cc) solutions, which is distinguished by smaller bubble production, spread over a wider portion of the heater surface with the entire range of heat fluxes considered in the experiments. There is reduced coalescence of bubbles that have a higher departure frequency, both outcomes of reduced liquid-vapor interfacial tension. Also, molecular physisorption of the polymer on the heater surface may contribute to the formation of new sites [21, 58, 67], which would perhaps account for the increase in number of nucleation sites despite a slight increase in the surface wettability (as indicated by the small reduction in contact angle shown in Fig. 8).

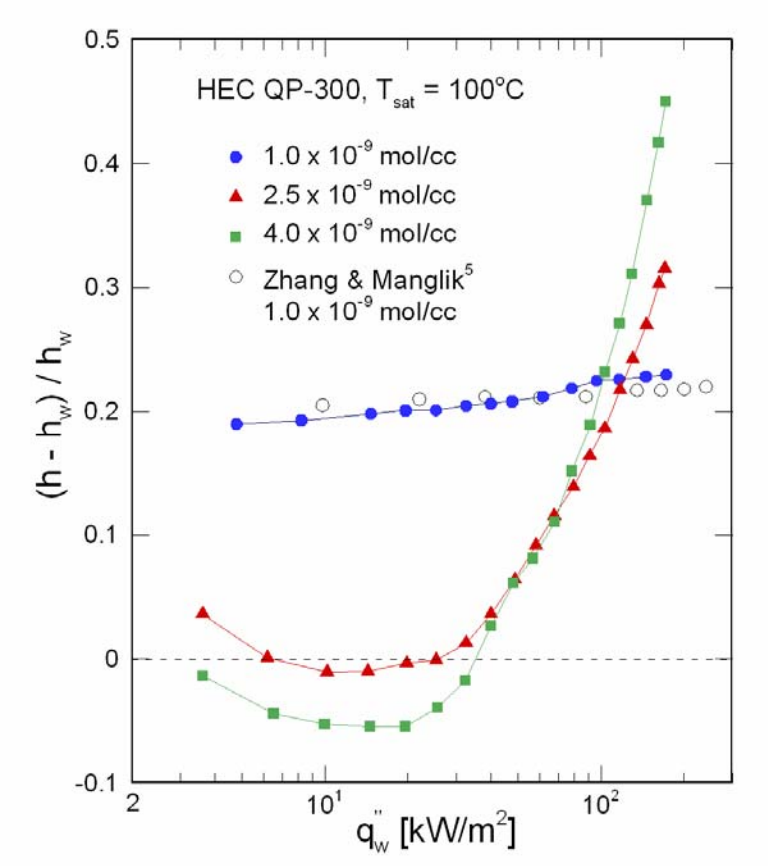

Figure 10. Variation of enhancement in boiling heat transfer coefficient with wall heat flux in different concentrations of aqueous HEC QP-300 solutions.

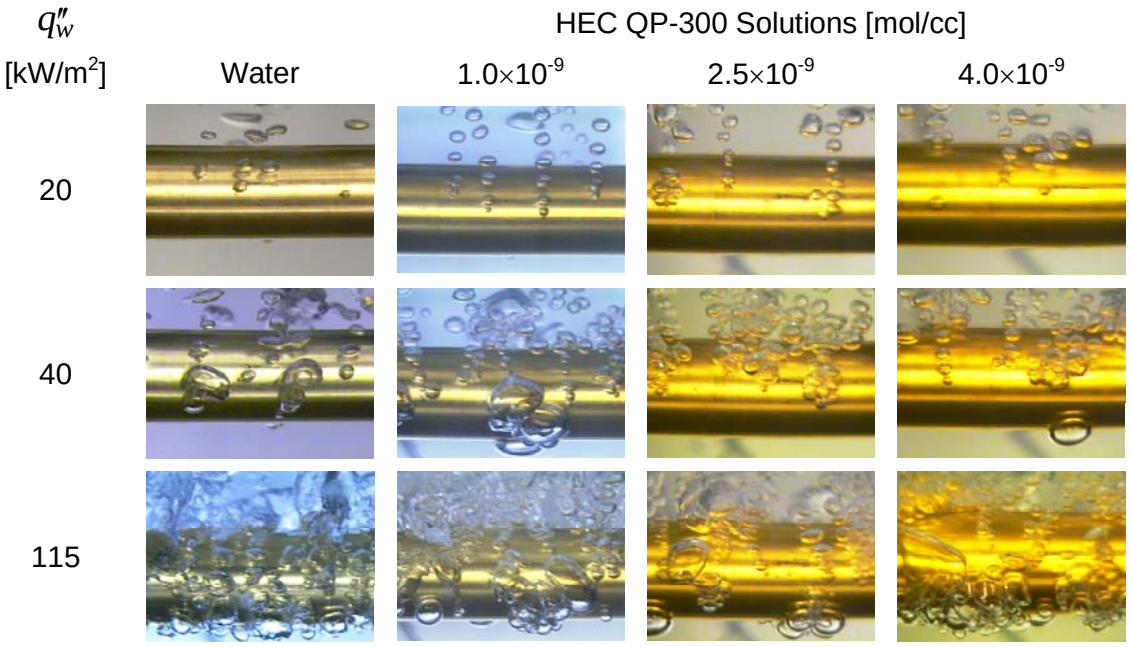

Figure 11. Ebullient or bubbling behavior during boiling of pure water and aqueous solutions of HEC QP-300 in different molar concentrations.

However, in the larger concentration solutions ($C > C^*$, or $C = 2.5\times10^{-9}$ and 4.0×10^{-9} mol/cc) and at low heat fluxes (q''_w = 20 kW/m^2, or the partial boiling regime), the extent of bubbling activity decreases substantially (Fig. 11). This is possibly due to the increased viscosity of the higher concentration polymer solution, as seen in Fig. 4, where the zero-shear rate viscosity η_o increases as $1.35\times10^{-3} \rightarrow 2.1\times10^{-3} \rightarrow 3.2\times10^{-3}$ N·s/m^2 or about ~ 1.6×-to-2.4× that at C^*. The consequent higher viscous drag at the dynamic vapor-liquid interface tends to suppress or retard the post-nucleation growth of vapor bubbles. This then leads to increasing deterioration of boiling performance with polymer concentration C at lower heat fluxes. The relatively higher shear rate associated with greater vapor generation when $q''_w \geq 40$ kW/m^2, on the other hand, lowers the viscosity of the shear-thinning or pseudoplastic solutions. With the attendant reduction in viscous retardation at the vapor-liquid interface re-establishes the dominance of

interfacial tension relaxation of higher concentration polymeric solution, and the bubbling activity again increases. The shear thinning behavior is more pronounced in the $C = 4.0\times10^{-9}$ mol/cc solution, thereby further intensifying the ebullience and the boiling heat transfer.

Conclusions

That different bulk concentrations of the polymer additive HEC QP-300 in water anomalously alter the nucleate boiling heat transfer performance is evident from the results presented in Figs. 9-11. The primary controlling influence is rendered by the rheology of the solution, which ranges from a highly viscous behavior to shear-thinning characteristics with increasing shear rates. Both the viscous nature and pseudoplasticity in turn increase with the polymer concentration, and this diversely affects the different boiling regimes; in the partial boiling, low-frequency bubble-generation regime the viscous behavior dominate, whereas in the fully developed, high-frequency bubble-generation regime the shear-thinning behavior of the polymeric solution has greater influence. Furthermore, the reduction in dynamic surface tension (which alters the required superheat for the onset of boiling and post-departure bubble frequency), and possibly the macromolecular physisorption of the polymer onto the heating surface (which perhaps aids the formation of new nucleation sites) are also the controlling factors for the boiling heat transfer enhancement in lower the concentration ($C \sim C^*$) solution.

Improvements in the boiling performance, varying from 19% – 22% increase in the heat transfer coefficient relative to that in pure water, were obtained with $C = 1.0\times10^{-9}$ mol/cc over the entire heat flux range of the experiments. On the other hand, the reduction in nucleate boiling heat transfer coefficients with higher concentrations ($C > C^*$) at low heat flux levels is caused by the retardation of vapor-bubble growth and post-departure bubble frequency, possibly

due to the viscous suppression of micro-convection in the bubble boundary layer. This decreased ebullience, observed in the partial boiling regime, is reversed and augmented at higher heat fluxes (q''_w > 40 kW/m^2) where the higher shear rate at vapor-liquid interfaces of bubble that are more vigorously produced lends to a shear-thinning viscous behavior in the solution. The enhancement in the fully developed boiling regime produces a peak performance when q''_w > 100 kW/m^2, and up to 45% increase in the boiling heat transfer coefficient, compared to that in pure water, is obtained with $C = 4.0\times10^{-9}$ mol/cc.

Nomenclature

A cylindrical heater surface area, $2\pi r_o L$ [m^2]

C concentration [mol/cc]

C^* critical polymer concentration or overlap concentration [mol/cc]

g gravitational acceleration [m/s^2]

h heat transfer coefficient [W/m^2·K]

h_w heat transfer coefficient of water [W/m^2·K]

I current [A]

K consistency index, Eq. (4) [N·s^n/m^2]

k_1 constant in Einstein's viscosity model, Eq. 5 [-]

L heated length of cylindrical heater [m]

l_c capillary length, $\sqrt{\sigma/\rho g}$ [m]

M molecular weight [kg/mol]

n flow behavior index, Eq. (4) [-]

p pressure, [N/m^2]

q''_w heat flux [kW/m^2]

R_p average surface roughness of heater, Fig. (3), [μm]

r radius of embedded thermocouple location in cylindrical heater, Eq. (2) [m]

r_o outer radius of cylindrical heater surface [m]

T_w temperature of heater surface [K]

T_{sat} saturation temperature of test liquid pool [K]

ΔT_{sat} wall superheat or wall-to-pool temperature difference, $\left(T_w - T_{sat}\right)$ [K]

V voltage [V]

ϕ volume fraction of spherical particles in dilute dispersions [-]

$\dot{\gamma}$ shear rate [s^{-1}]

η viscosity and/or apparent viscosity of polymeric solution [N·s/m^2]

$[\eta]$ intrinsic viscosity [dl/g]

η_o zero shear-rate viscosity of polymeric solution [N·s/m^2]

η_{rel} relative viscosity, $\left(\eta/\eta_s\right)$ [-]

η_s viscosity of solvent [N·s/m^2]

η_{sp} specific viscosity, $\left(\eta - \eta_s\right)/\eta_s$ [-]

ρ liquid density [kg/m^3]

σ surface tension [N/m]

τ surface age of bubble [s]

EFFECTS OF INTERFACIAL PROPERTIES ON NUCLEATE POOL BOILING IN WATER-SURFACTANT SOLUTIONS

Introduction

Pool boiling is an efficient mode of heat transfer in which a relatively small temperature difference results in high heat transfer rates [62, 63, 91, 92]. Several reviews have documented the use of active and passive techniques for enhancement of nucleate boiling heat transfer. Among these, the use of surface active additives, which include surfactants and polymers that alter the surface tension of the boiling liquid even at very low concentrations, has been the focus of some current research [5, 6, 23-25, 93-95]. Much of the changes in boiling behavior have been attributed to the dynamic variations in surface tension, wetting or contact angle, and viscosity that influence and control the bubble dynamics in phase change [6].

Of the many different reagents considered in the literature for altering boiling heat transfer, surfactants are perhaps the most effective. They are long-chain molecules with a structure that is made up of a hydrophilic head and a hydrophobic tail. They adsorb at the liquid-vapor interface with their polar head towards the aqueous region and the hydrocarbon tail directed towards the vapor [27]. They are broadly classified on the nature of the hydrophilic part of the molecule as anionics, nonionics, cationics, and zwitterionics. Their adsorption at liquid-vapor interfaces causes local surface tension relaxation, and that at liquid-solid interfaces alters wetting. These are diffusion rate dependent processes, which are controlled by the reagents' diffusion-adsorption kinetics, micellar dynamics, ethoxylation, and bulk concentration levels [27, 35]. The change in interfacial tension and heater surface wetting can significantly alter the bubble dynamics (inception, growth, and frequency of departure) and thereby the heat transfer in

nucleate boiling [6]. Most often, with a characteristic range of concentrations of a given surfactant, the heat transfer has been found to be enhanced considerably when a characteristic range of concentration of a given surfactant is used in the solution [43]. The optimal or peak enhancement tends to occur at the critical micelle concentration of the reagent.

This critical micelle concentration or CMC is a unique concentration of the reagent or colloid-size clusters above which micelles are spontaneously formed in solution. The surface tension of the solution decreases continually with increasing surfactant concentration till CMC, beyond which an asymptotic constant surface tension is attained. This is driven by the adsorption-desorption dynamics at the gas-liquid interface, and is functionally dependent upon the bulk concentration and surface age of the interface [6, 25, 35, 42, 43]. Much of the increment in boiling heat transfer has been attributed to the surface-age and concentration dependent surface tension relaxation; surface wetting alters nucleation and liquid quenching of the heater surface. It is hypothesized that dynamic surface tension effects and the reagent's molecular dynamics perhaps scale the heat transfer coefficient in nucleate pool boiling.

The objective of this study is to explore the effects of changes in dynamic vapor-liquid interfacial tension on nucleate pool boiling performance of aqueous surfactant solutions. An amphoteric fluorosurfactant FS-50 (product of DuPont) is used in distilled, de-ionized water solutions, which produces very low surface tension in micellar and higher concentrations. The interfacial properties of FS-50 solutions in various concentrations are recorded to establish the interface adsorption kinetics of this relaxation behavior. Saturated pool boiling heat transfer at atmospheric pressure is measured in a controlled set of experiments with an electrically heated, horizontal cylindrical heater, by the variation of the applied wall heat flux q'' with wall superheat ΔT_{sat}. The presented results characterize ebullient phase change heat transfer from incipience or

onset of nucleate boiling (ONB) to the fully developed nucleate boiling regime, and the effects of dynamic interfacial relaxation on the heat transfer are delineated.

Experimental Methods and Materials

Boiling experiments

Figure 1a shows the experimental apparatus for nucleate pool boiling measurements. It consists of two large glass vessels, of which the inner tank holds the surfactant solution and the heater while the outer tank provides an insulating casing where silicon oil (50 cSt) is circulated to reduce heat loss and maintain the test pool at saturation temperature. Neslab's RTE-221 oil bath, which was heated to ~135°C, well above the saturation temperature of water, so as to form a thermal jacket around the test pool. Also, to ensure a constant liquid pool level at atmospheric pressure, the generated vapor was condensed over a water-cooled reflux condenser, mounted atop the pool; an additional coiled-tube condenser was used at high heat fluxes and much greater vapor generation. An auxiliary heater was used to quickly heat the pool to saturation temperature. A simple U-tube manometer, mounted on the top of the inner vessel, monitored the pool pressure with a ±0.001 atm (or 5 mm of water column) accuracy throughout the pool boiling experiments.

The heating test section (shown in Figure 1b) consists of a horizontal, gold plated, hollow copper cylinder of 22.2 mm outer diameter; the 0.0127-mm thick gold plating mitigates any surface degradation and oxidation from chemicals in the test fluids. A 240 V, 1500 W cartridge heater, with hermetically insulated lead wires, is press fitted in the hollow cylinder with thermally stable conductive grease to fill any remaining air gaps and pockets of thermal resistance. It is centrally located inside the copper tube, and the gaps at each end are filled with

silicone to prevent water contact. The heater-wall and pool-bulk temperature measurements were made with precision (±0.5°C) copper-constantan thermocouples, connected to a computerized data acquisition system with an in-built ice junction and calibration curve. A variac-controlled AC power supply, a current shunt (0.15 Ω with 1% accuracy), and two high-precision digital multimeters for current (±2.5% accuracy) and voltage (±1.5% accuracy) were used to record the input electric power and thus determine the heat load.

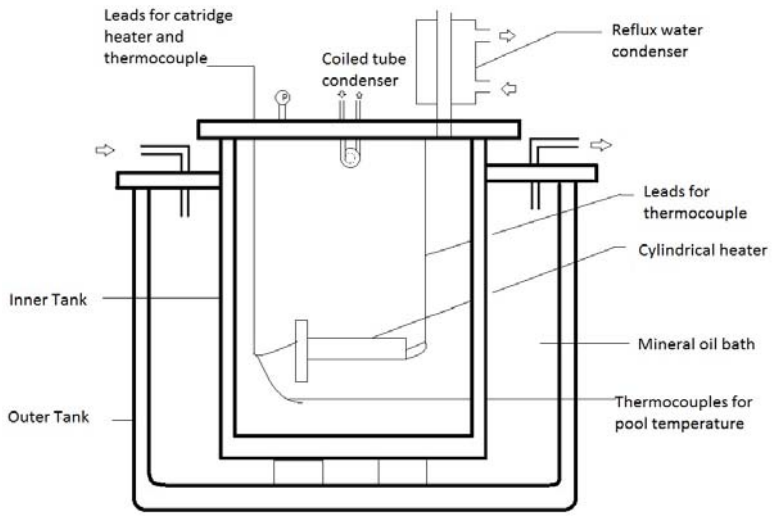

(a)

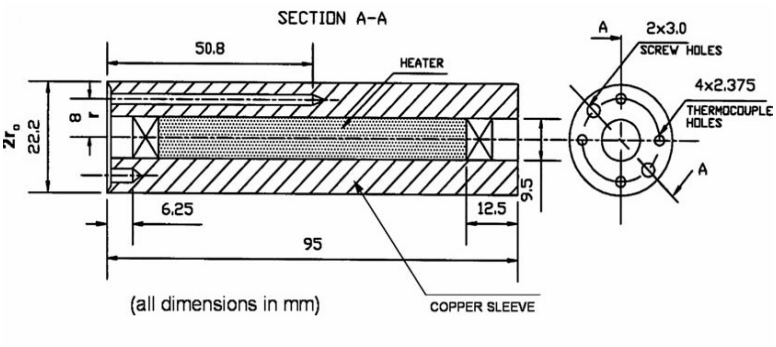

(b)

Figure 1. Experimental apparatus: (a) schematic of pool boiling set up, and (b) constructional details of cylindrical heater assembly.

At each incremental value of power input or heat load, the dissipated wall heat flux was computed from the measured voltage V, current I, and heater surface area A (= $2\pi r_o L$; where L is the length of heated heater) as,

$$q'' = \left(V \cdot I / A\right) \tag{1}$$

In these calculations, the actual voltage drop across the heater and the actual current flowing through it (measured directly across the precision shunt resistance in series with the heater) were recorded directly to provide the actual heat load, which inherently calibrates for any temperature-dependent variations in resistance [70, 71]. The wall superheat ΔT_{sat} for this heat flux was determined from the heater-wall temperature ΔT_w, taken as the average value of three wall-temperature thermocouples reading ($T_{i,r}$) that are embedded in the heater surface, and the saturation temperature T_{sat} of the liquid pool as follows:

$$T_w = \left[\frac{1}{3}\sum_{i=1}^{3}\left\{T_{i,r} - \left(q'' r_o / k\right)\ln\left(r_o / r\right)\right\}\right] \tag{2}$$

$$\Delta T_{sat} = \left(T_w - T_{sat}\right) \tag{3}$$

In Eq. (2), r is the radius of wall thermocouple location, r_o is the heater's outer radius, and k is the thermal conductivity of heater material. The maximum experimental uncertainties in q'' and ΔT_{sat} were calculated by the single-sample propagation of error method [72] to be ±2.92% and ±0.33%, respectively.

At the start of every experiment, the pool was thoroughly degassed by first heating it to the saturation temperature by using the auxiliary heater, and then boiling it at a low heat flux while constantly maintaining it at T_{sat}. The auxiliary heater was then shut off and the system was allowed to attain equilibrium. The whole process took about two to three hours to complete.

Once the pool was thoroughly degassed, the boiling experiments were carried out by increasing the voltage across the cylindrical heater in incremental steps, and measuring the power along with the temperature of the pool and heated surface after equilibrium was attained. Photographic records were taken at every increment of voltage to observe any changes in the ebullient behavior. Multiple boiling runs were taken with distilled water to ensure accuracy and repeatability. These results are presented in Fig. 2, where the pure water boiling data are seen to be in good agreement with some previous data [25], and are also within the envelope of predictions given by the much cited Rohsenow [73], Borishanskii [74], Cooper [75], and Cornwell and Houston [76] correlations. This validates the data acquisition methods and provides the baseline water results for evaluating and contrasting the boiling performance of aqueous surfactant solutions.

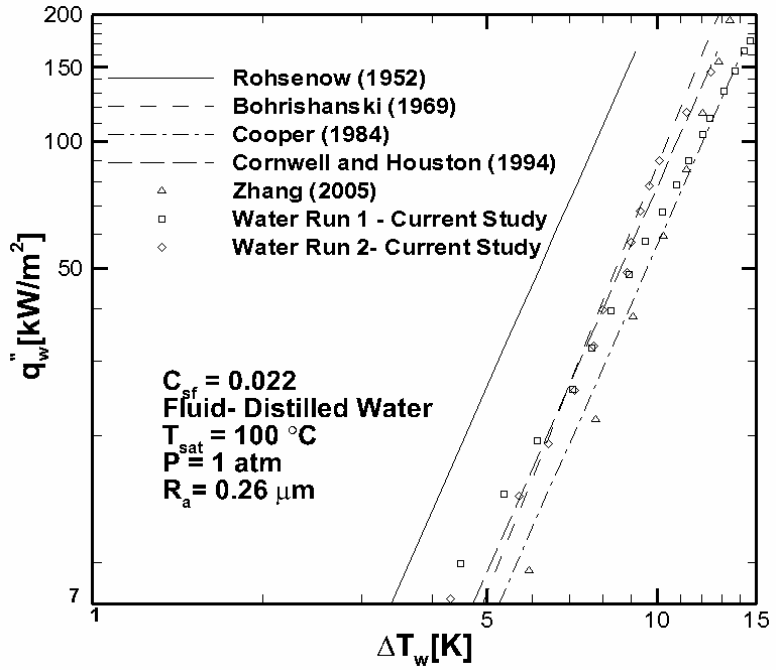

Figure 2. Nucleate pool boiling results for de-ionized distilled water and comparison with several correlations.

Photographic Record of Boiling

A PULNix TMC-7 series high-speed CCD camera was used to capture the visual dynamics of bubble generation, growth, and the motion during boiling. It has a digital resolution of 768 (horizontal) × 494 (vertical) pixels, with eight different shutter speeds that go up to 1/10,000 sec. The camera is also fitted with FUJI 12.5-mm × 75-mm zoom lens for capturing close-up photographs during different stages of boiling. The camera was interfaced with a PC using a USB-based digital image capture and processing system (DQP-A4 premier), which records consecutive frames of video in real-time images at 60 frames/s.

Surface Tension Measurements

A SensaDyne QC6000 tensiometer was used to measure the equilibrium and dynamic surface tension of surfactant solutions which operates on the maximum bubble pressure method. Two glass capillaries of unequal diameters are immersed in the test fluid pool in a beaker. The test fluid is maintained at a constant temperature, which is measured using a well calibrated thermistor (±0.1°C precision) attached to the orifice probes. When dry air is bubbled through the orifices, a differential pressure signal is produced, which is proportional to the gas-liquid interfacial tension. Also, the time interval between the newly formed interface and the point of bubble break-off at the orifice mouth is referred to as the surface age τ of the interface. It gives the measurement of bubble growth time that corresponds to the dynamic surface tension value at a given operating bubble frequency. Thus, by altering the air-bubble frequencies through the probes, both equilibrium and dynamic surface tension can be measured; the equilibrium data are obtained at very high surface ages that lead to static conditions. Details of the calibration and measurement validation procedures are given in [35]. The maximum uncertainties in solution

concentration, temperature, and surface tension measurements were found to be ±0.4%, ±0.5%, and ±0.7%, respectively.

Results and Discussion

The fluorosurfactant FS-50 in aqueous solution produces a very large interfacial tension relaxation with increasing concentrations. The variation of equilibrium surface tension, or liquid-vapor interfacial tension, with varying concentration is graphed in Fig. 3. It is seen to decrease continually from that of water (σ = 72.5 mN/m) to a minimum asymptotic value of σ = 18.4 mN/m. The concentration that corresponds to the lower inflection point in the $\sigma - C$ isotherm gives the critical micelle concentration or *cmc* of the surfactant [35]. This concentration marks the onset of spontaneous formation of miscelles in the solution, and beyond which surface tension does not show any further decrement. From Fig. 3 the *cmc* of FS-50 is estimated to be around 1400 wppm.

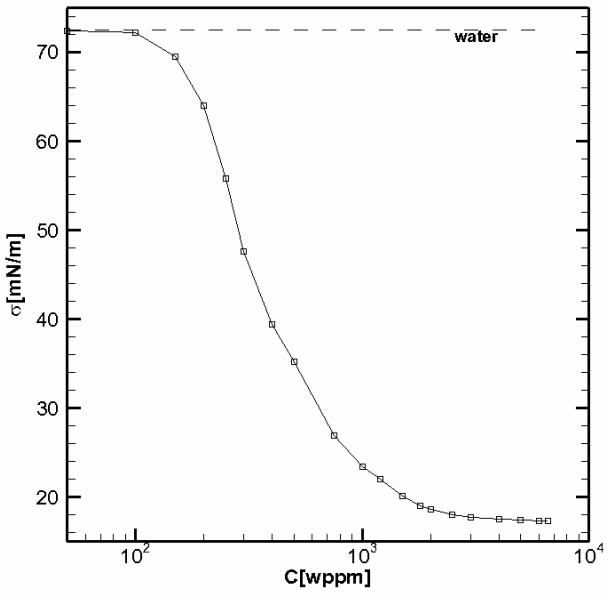

Figure 3. Equilibrium gas-liquid interfacial tension (surface tension) and its variation with surfactant concentration in aqueous solution.

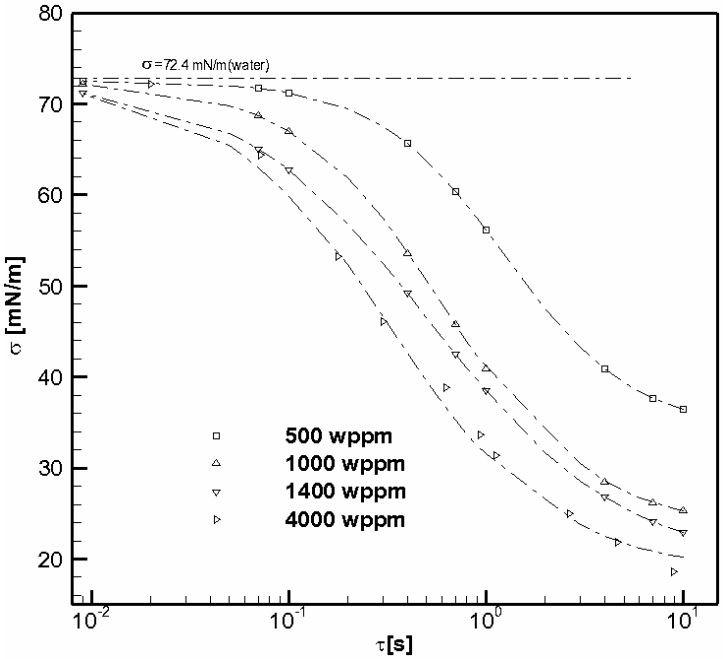

Figure 4. Temporal variation of dynamic surface (gas-liquid interfacial) tension for different concentration of FS-50 in aqueous solutions.

Furthermore, the liquid-vapor interfacial tension is a time-dependent process, and the graph for σ versus τ in Fig. 4 depicts this time dependence of the interfacial tension. It can be seen that a finite time ($\tau >$ 8-10 s, depending upon *C*) is needed for complete interface-tension relaxation, or to attain equilibrium at the gas-liquid interface with the bulk concentrations. For $\tau <$ 30 ms, the interfacial tension is essentially the same as that of the solvent. The time-scale region 30 ms $< \tau <$ 8 s, however, is marked by very sharp decrease in σ. It is this gradient that characterizes the dynamic surface tension behavior at the evolving liquid-vapor interface [6, 50, 89], and has been attributed to the modification of ebullience and boiling [6, 25]. It may be noted that the time-dependent adsorption isotherm fit through the data in Fig. 4 has been graphed by the method outlined by Hua and Rosen [89].

Nucleate pool boiling is fundamentally a complex process involving the interplay of various interfacial forces associated with surface tension, heater surface wetting and liquid rheology.

The wetting of the heater surface controls nucleation and its site density, while surface tension alters the post-nucleated bubble dynamics [6, 25]. In aqueous surfactant solutions, these properties vary with additive concentration and with time, and the consequent effects on nucleate pool boiling are described by the boiling curves of Fig. 5. The leftward shift in the curves for different aqueous solutions shows the extent of heat transfer enhancement with varying surfactant concentration. The heat transfer enhancement is seen to increase with surfactant concentration, and a peak or maximum improvement is attained when $C = cmc$, i.e., with the critical micelle concentration. However, with concentrations higher than *cmc*, boiling augmentation decreases considerably. This behavior concurs with the findings in some other studies with anionic, cationic, and non-ionic surfactants [23-25]. In fact, in the later case, the boiling performance has been found [23-25] to even deteriorate below that of the solvent in aqueous solutions with $C > cmc$.

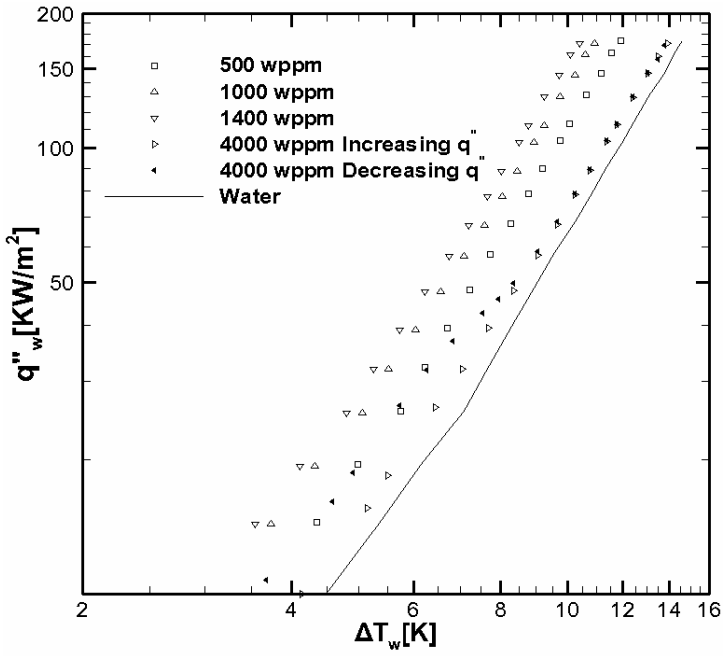

Figure 5. Nucleate pool boiling data for different concentrations of aqueous FS-50 solutions, along with that for distilled de-ionized water.

The variation of the enhanced heat transfer coefficient, quantified by the dimensionless ratio $[(h - h_w)/h_w]$ with surfactant concentration C in solution, for the heater wall heat flux of 150 kW/m^2 is graphed in Fig. 6. It gives clear evidence of the peak enhancement in heat transfer with $C = cmc$, which can be perhaps related to the sharp decrease in σ with respect to both C and τ in FS-50 solutions. Up to 45% increase in boiling heat transfer coefficient is obtained, which is comparable to the 25% to 65% peak enhancement reported in previous studies [23, 24]. The photographic records of boiling at the comparable wall heat flux of 110 kW/m^2 presented in Fig. 7, provide additional insights and depict the differences in the ebullience at different solute concentrations. Compared to bubble generation in pure water, increasingly smaller bubbles and in much higher surface density are seen to be produced as C = 500 wppm $\rightarrow$ 1400 wppm (= cmc). In a solution with $C > cmc$ (4000 wppm), though the extent of bubbling activity appears to be more vigorous, it is accompanied with vapor blanketing of swaths of heater surface. This reduces the heat transfer considerably, as is also reflected in the quantification of Fig. 6.

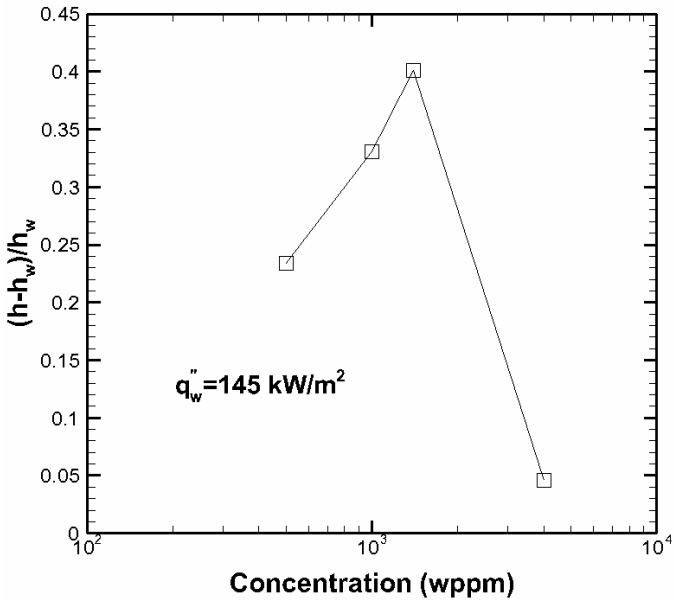

Figure 6. Variation of boiling heat transfer coefficient with concentration of FS-50.

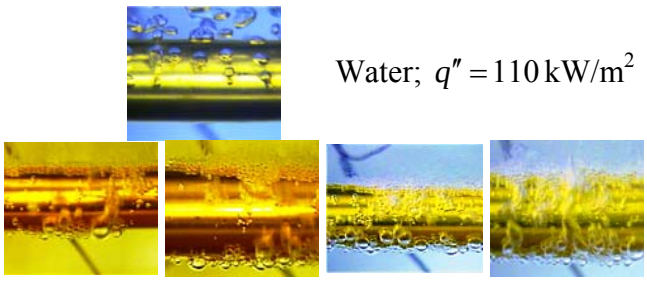

Figure 7. Ebullient or bubbling behaviour in boiling of deionized distilled water and different concentration aqueous FS-50 solutions.

Conclusions

Boiling behaviour of water is altered considerably by the addition of FS-50 fluorosurfactant as evident by Figs. 5-7. The controlling feature is rendered by the interfacial tension change of the solution, which ranges from a very low value of equilibrium surface tension to the surface tension of water (solvent). This is both a solute bulk-mass- and time-dependent process. The surface tension relaxation increases with concentration of the surfactant in solution. This affects the different boiling regimes. In the partial boiling, low frequency bubble-generation regime, the equilibrium values of surface tension play an important role; whereas in high heat flux boiling with greater bubble frequencies, the dynamic changes in surface tension dominate. Thus, the dynamic behavior of interfacial tension perhaps controls the boiling performance in FS-50 fluorosurfactant aqueous solutions.

Improvements in the boiling performance, varying from 40% – 45% increase in the heat transfer coefficient, relative to that in boiling of pure water, were obtained with C = 1400 wppm (~ *cmc* of FS-50 in water) over the entire heat flux range in the experiements. On the other hand, the reduction in the enhancement of nucleate boiling heat transfer with higher concentrations of $C > cmc$ at low heat flux levels is caused by the retardation of vapor-bubble growth and post-

departure bubble frequency. This altered boiling behavior is found to relate well with the observed changes in interfacial tension. Peak performance in boiling is obtained at lower heat fluxes where a lesser (equilibrium) surface tension plays a more dominant role than the dynamic surface tension. At higher heat fluxes, the heat transfer coefficient relative to water decreases when the dynamic behaviour of surface tension plays a more important role.

Nomenclature

A heater surface area ($= 2\pi r_o L$) [m^2]

C concentration [wppm]

cmc critical micellar concentration [wppm]

h boiling heat transfer coefficient [$kW/m^2 \cdot K$]

I current [A]

k thermal conductivity of heater material [$kW/m \cdot K$]

L length of heated cylinder [m]

q'' heater-wall heat flux [kW/m^2]

l_c capillary length [m]

r radius of wall thermocouple location [m]

r_o cylindrical heater outer radius [m]

T temperature [K]

ΔT_w wall superheat ($T_w - T_{sat}$) [K]

V voltage [V]

σ surface tension [mN/m]

Subscripts

o	at outer surface
r	at radial location
sat	at saturation condition
surf	pertaining to aqueous surfactant solution
w	at heater wall
water	pertaining to pure water

SINGLE-BUBBLE DYNAMICS IN ISOTHERMAL LIQUID POOLS: EFFECTS OF FLUID PROPERTIES, ORIFICE DIAMETER AND FLOW RATE

Introduction

Adiabatic single bubble dynamics provides a fundamental basis for understanding variety of thermal and hydrodynamic transport processes with ebullient gas-liquid interfaces. These include aeration, fermentation, waste-water remediation, bio-chemical transformation, and ebullient phase-change, among others. The rather complex gas-liquid interactions in bubble formation at the tip of an orifice in a liquid pool are primarily governed by a balance of several lifting (aiding) and restraining (retarding) forces. As schematically represented in Fig. 1, and for a system in a gravitational environment, the bubble growth is aided by gas momentum, pressure and buoyancy forces, which are in turn constrained by the forces due to inertia, viscous drag, and surface tension. These forces that govern the dynamic behavior of bubbles are dependent on the volumetric flow rate of the gas, orifice size, and physicochemical properties of the fluid, which essentially influence the contact time between the two phases [22, 96].

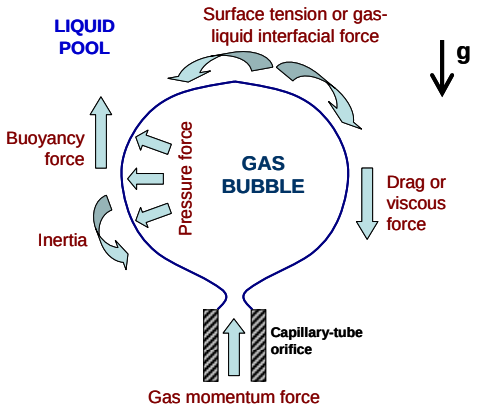

Figure 1. Schematic of interfacial force balance that governs the dynamics of an evolving gas bubble in a liquid pool.

Single-bubble dynamics has received considerable attention in literature [22, 96-98], and numerous experimental as well as theoretical or computational investigations have explored the effects of various parameters on the behavior of adiabatic gas- bubbles that are formed at the tip of a submerged orifice in isothermal liquid pools. Kulkarni and Joshi [96] provide a more recent and extended review documentation of this body of work. In one of the earliest investigations dating back to 1941, Eversole et al. [98] used nitrogen gas and a glass orifice in water and alcohol, and found the bubble size to be dictated only by gas flow rate. Later, in 1950, van Krevelen and Hoftijzer [99] applied the simple Tate's law [100] to balance buoyancy with surface tension to estimate the bubble departure diameters in an air-water system. With a series of parametric experiments, Datta et al. [101] suggested two regimes of bubble formation that are determined by flow rate and orifice diameter. At low flow rates and for a given orifice size, the bubble size is constant and independent of $\dot{Q}$ though the bubbling frequency changes proportionally. With higher flow rates, on the other hand, the bubble size was found to first decrease, reach a minimum, and then increase. They also observed that I in both the bubble regimes the hydrostatic head had little influence on the interplay between bubble formation rate and its size.

Benzing and Myers [102] subsequently characterized these two bubble-formation regimes on the basis of the formation frequency as *static* and *growth* regimes. Furthermore, they found the bubble departure diameter to be independent of gas properties and liquid viscosity in the *static-bubble* regime, and could predict their own data by the following correlation:

$$d_b = 1.82\left(\sigma d_o^3 / g\rho_l\right)^{1/4} \tag{1}$$

Davidson and Amick [103] also observed the two-regime bubble-formation behavior in experiments with water and mineral oil using a number of different orifice plates. For higher flow rates they proposed a correlation for predicting the bubble volume $\left(Q_b = \pi d_b^3/6\right)$ that can be restated

$$d_b = 0.59\left(\dot{Q}\sqrt{d_o/2}\right)^{0.289} \tag{2}$$

It was also found that the container width and submerged depth of orifice had no effect on the bubble size. Calderbank [104] has reported that above a certain gas flow rate, the frequency of bubble formation was nearly constant and independent of gas flow rate, slot dimensions, and physical properties of both liquid and gas. Based on another set of air-water experiments, Davidson and Schuler [105] suggested that the bubble volume depended only on the flow rate and was independent of the surface tension in the static bubble regime.

There have been limited efforts to develop generalized equations to predict bubble departure diameters, which is not surprising given that large parametric variability in data and their determinants. One of the more frequently cited correlation [96] is that reported by Tadaki and Maeda [106]. Based on data for different fluids, orifice diameters, and gas flow rates which were scaled by Weber and Froude numbers, the following two equations are given for the *static* and *growth* regimes, respectively:

$$d_b = \left[\frac{\sigma d_o}{g\rho_l}\left(6 + 2.5\frac{\mathrm{We}}{\sqrt{\mathrm{Fr}}}\right)\right]^{1/3} \qquad \left(\mathrm{We}/\sqrt{\mathrm{Fr}}\right) < 16 \tag{3}$$

$$d_b = \left[1730\left(\frac{\sigma d_o}{g\rho_l}\right)\right]^{1/3}\left(\frac{\sqrt{\mathrm{Fr}}}{\mathrm{We}}\right)^{1/9} \qquad \left(\mathrm{We}/\sqrt{\mathrm{Fr}}\right) < 16 \tag{4}$$

Interestingly, a potential-flow-theory-based model for the calculation of departure bubble volume and bubbling frequency from a submerged orifice was proposed by Kupferberg and

Jameson [107]. This was supported by limited experiments with air-water and air-ethanol ebullience. However, under similar operating conditions, the volume of bubble formed in water was larger than that in ethanol, and this discrepancy was attributed to the effect of the liquid inertia (deviation from potential flow) on the bubble growth rate. To support yet another two-stage, inviscid-fluid, potential-flow-theory-based model, Wraith [108] found his own data with plate orifices made of brass and Perspex in an air-water system at high flow rates to be in fair agreement with the predictions from

$$d_b = \left(6.54\dot{Q}^{6/5}/\pi g^{3/5}\right)^{1/3} \tag{5}$$

In a different approach and a semi-empirical analysis, where the bubble neck length at detachment was assumed to be (d_b/4), on the basis of experimental data reported by Räbiger [109] to evaluate the bubble centerline velocity, Gaddis and Vogelpohl [110] have proposed the following rather cumbersome and implicit correlation.

$$d_b = \left[\begin{array}{c} \dfrac{6d_o\sigma}{\left(\rho_l-\rho_g\right)g}\left(1-\dfrac{\mathrm{We}}{4}\right)+\left\{\dfrac{81\mu\dot{Q}}{\pi\left(\rho_l-\rho_g\right)g}\right\}\dfrac{1}{d_b} \\ +\left\{\left(\dfrac{135}{4\pi^2}+\dfrac{27\rho_g}{\pi^2\rho_l}\right)\dfrac{\rho_l\dot{Q}^2}{\left(\rho_l-\rho_g\right)g}\right\}\dfrac{1}{d_b^2} \end{array} \right]^{1/3} \tag{6}$$

The review by Kulkarni and Joshi [96] has compared the results of different models and correlations with experimental data to suggest that the Gaddis and Vogelpohl [110] is perhaps the most suitable for predicting bubble departure diameter. However, as shown later in this paper, this as well as the correlation by Tadaki and Maeda [106] fail to adequately predict bubble growth at low flow rates from smaller diameter orifices.

Though gas-bubble formation in isothermal liquids is influenced by several variables, not all of them influence the ebullient behavior to the same extent [111]. As discerned from the

previous literature, there are many gaps in our understanding of the influence and scaling of different parametric determinants. Furthermore, not much attention has been focused bubble formation transients (frequency or bubble interval, and the time taken to grow from inception to departure or growth time). Because the interfacial area, which is influenced by the contact time between gas-liquid phases, significantly controls the mass-transfer process, characterizing the hydrodynamics of bubble departure diameter, growth time, and bubbling interval are critical to the development of generalized scaling and correlation. This work addresses these issues with a systematic experimental study of adiabatic air-bubble ebullience, where the effects of fluid properties, orifice diameter, and air-flow rate on the dynamics of bubble formation has been examined. Five different test liquids (water, ethanol, propylene glycol, and glycerol, which represent a broad spectrum of liquid surface tension and viscosity, but nearly the same density) were employed, along with three different submerged capillary-tube orifices (d_o = 0.32, 1.0, and 1.76 mm) and a range of air-flow rates ($2 \leq \dot{Q} \leq 20$ ml/min) in the *static-bubble* regime. The results for temporal variations of bubble volume with flow rate and time (growth time from inception to departure, and bubble interval or frequency) as well as photographic images of bubble growth dynamics are presented. A scaling analysis is also presented in an effort to correlate the bubble departure diameter with flow rate, orifice diameter, and fluid properties.

Experimental Setup and Method

The experimental setup for generating air bubbles from a submerged capillary orifice in an unheated, isothermal pool of water and recording the ebullient dynamics in real time is schematically depicted in Fig.2. A quiescent pool of distilled and de-ionized water was maintained at room temperature (23^oC) in a circular 4000 ml glass tank of 161.4 mm diameter.

Bubbles were generated by blowing controlled amount of compressed air through a hypodermic needle submerged vertically at the bottom of the pool; capillary needles of three different diameters (d_o = 0.32 mm, 1.0 mm, 1.76 mm) were used. Air at constant flow rate was supplied and controlled through a syringe pump. The needle orifice tips were submerged to a depth of 80 mm for all experiments. A high-speed high-resolution digital camera with a computer interface was used for real-time image capture, and the videography was analyzed digitally.

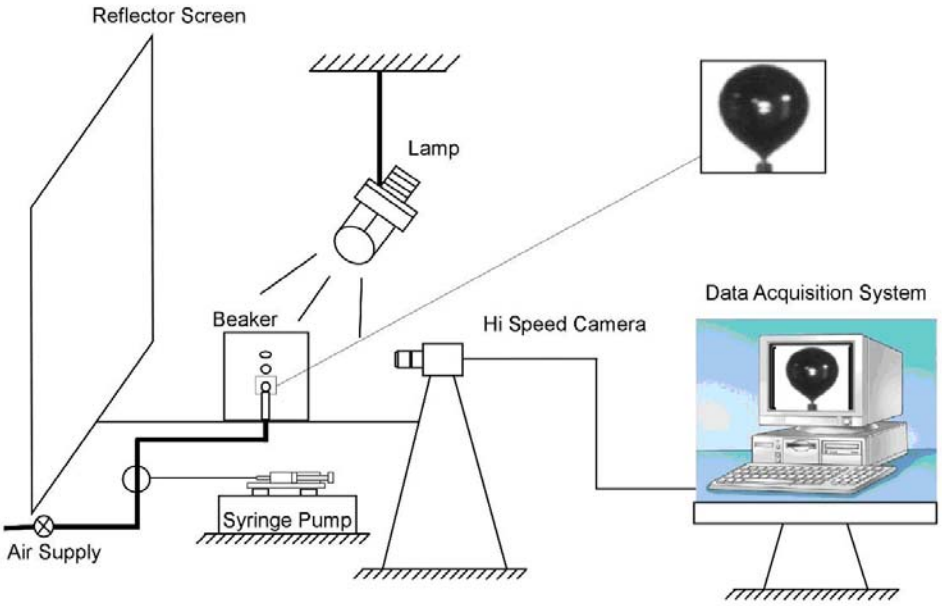

Figure 2. Schematic diagram of the experimental set up

Data for bubble shape, size, time of growth (period between embryonic nucleation and detachment), and generation frequency were acquired through precision, high-speed, high resolution flow visualization and digital image processing. The digital camera system (Hi-DCam II version 3.0 - NAC Image Technology) was set normal to the orifice tip so as to obtain a frontal view of the growing and departing bubble. The frame rates were varied from 3000 fps and 4000 fps (corresponding shutter speed was 1/frame speed), and the 8× optical zoom lens of the camera

was focused at the orifice tip at a focal length of 1.75 ft. A focusing, single-ended, daylight PAR (parabolic aluminized reflector) lighting system along with a glossy white reflector was used for providing continuous lighting so as to obtain clear and sharply contrasted images of the bubble.

Sequential images of were recorded and analyzed frame-by-frame in image processing software (Image-Pro Plus 4.0; Media Cybernetics). The bubble interval was determined from the frame speed and recording the time elapsed between two consecutive photo frames for identical bubble detachment events at the orifice tip. Similarly, the bubble surface age was determined by calculating the time elapsed between photo-frames of bubble appearance at orifice tip to its departure. The equivalent diameter of the bubble at any stage of its growth was measured as the average of angular diameters measured at every 2^o angle (i.e., 180 different diameter measurements). These were based on a grey-scale (black and white contrast) saturation intensity calibration in the image processing software. The image of the capillary orifice and its outer diameter was used as the reference length for calibration which has a precision of 0.026 mm. The air flow rate was varied over a broad range ($2 \leq \dot{Q} \leq 20$ ml/min) to obtain a range of bubble formation rates or bubble intervals and air-flow Reynolds number spanning both the static and growing bubble regimes.

As stated earlier, the air-flow ebullience was observed in an isothermal, room temperature (23 ± 1^oC) pool of distilled and de-ionized water with physical properties as listed in Table 1. The precision in measuring bubble-interval and growth times was ±0.33ms and ±0.25 ms, respectively with 3000 fps and 4000 fps. Likewise, the bubble diameters could be measured to a ±0.026 mm precision based on the saturation intensity pixel density. Thus from a propagation error analysis, the maximum uncertainty in the measurement of the bubble diameter was found to be ±1.04% and that for air flow rate was ±1.0%.

Table 1. Physical properties of test liquids @ 23°C.

Liquid	ρ [kg/m^3]	σ [mN/m]	μ [kg/m·s]
Water	1027	72.1	0.911×10^{-3}
Ethanol	789	22.7	1.08×10^{-3}
Propylene glycol	1036	35.0	49.96×10^{-3}
Glycerol	1261	65.0	749.3×10^{-3}

Results and Discussion

The formation of single bubbles can be identified to fall into two regimes depending on the flow rate and orifice diameter. For a given orifice diameter and at low flow rates, the volume of bubble produced generally tends to be constant and independent of the gas flow rate [96, 101-103]. This is the *static-bubble* regime where the bubble size is depended only on the liquid properties and orifice size. At higher flow rates or in the *growth-bubble* regime, on the other hand, the bubble size increases with flow and is directly proportional to the gas flow rate and fluid properties. Only the static conditions are considered in this study. In this case, besides bubble *departure diameter* d_b, incipience, growth, and necking at departure from the tip the submerged orifice are also critical determinants and are characterized by the *growth time* τ_g and *bubble interval BI*. Growth time is the time elapsed between the initial bud formation to the final necking and departure, and bubble interval is the time period between two successive departures (or the inverse of bubble frequency or rate of formation). Furthermore, the difference between the bubble interval and the growth time is the *waiting time*. As one bubble departs, a new

interface is formed at the tip of the orifice. The gas flows continuously through the orifice causing pressure build up under the tip-liquid-film so as to overcome the retraining forces at the interface (surface tension and hydrostatic pressure). This causes the interface to bulge convexly to form the initial embryonic bubble, and the time taken for the gas pressure to achieve this is the waiting time.

The spatial-temporal evolution of air bubbles from the tips of submerged capillary-tube orifices in a quiescent isothermal pool of water is photographically depicted in Fig. 3. Typically the gas-bubble embryo initially grows rather slowly from a hemispherical shape to that of a spherical segment. Depending on the orifice size, almost 15% – 40% of the growth time is expended in this stage, where the gas flow to the interface essentially tries to overcome surface tension and inertial forces. This stage is followed by a rapid increase in rate of bubble formation as the buoyancy force begins to influence the interface more dominantly, and a mushroom-like profile is attained. With increasing gas supply the bubble shape extends to that of an inverted tear-drop at the orifice tip as necking and subsequent departure occurs. Viscous drag becomes significant in this stage and the bubble growth is retarded as it gets sheared at the neck above the orifice tip. Furthermore, the effective bubble diameter (volume-averaged) at departure is seen to be an increasing function of orifice size, and larger diameter orifices produce larger bubbles for the same gas flow rate in a given liquid.

That the ebullience considered in this study is in the *static-bubble regime* is clearly evident from Fig. 4. The shape and size of air bubbles at departure in water from a 0.32-mm orifice at different flow rates ($2 \leq \dot{Q} \leq 16$ ml/min) are depicted, and it is seen that $d_b \approx 2.51 - 2.52$ mm. Also, the growth time from embryonic inception to departure was constant ($\tau_g \approx 19$ ms), though the bubble interval decreased (or bubble frequency increased) with air-flow rate, and, as a

consequence, the gestation period or waiting time decreased considerably. This is seen in Fig. 5, where the change in the relative bubble diameter (d/d_o) with growth time τ_g normalized with the bubble interval is graphed for several different air-flow rates in water from d_o = 0.32 mm. A larger percentage of BI is vested in τ_g with increasing flow rate, while d_b remains about $0.8d_o$.

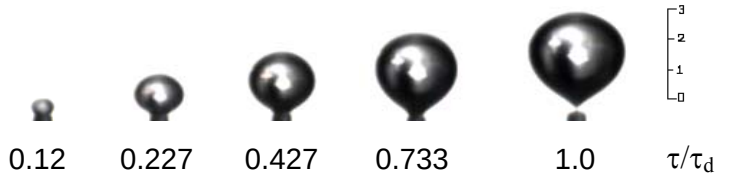

(a) d_o = 0.32 mm, d_b = 2.56 mm, τ_d = 34 ms

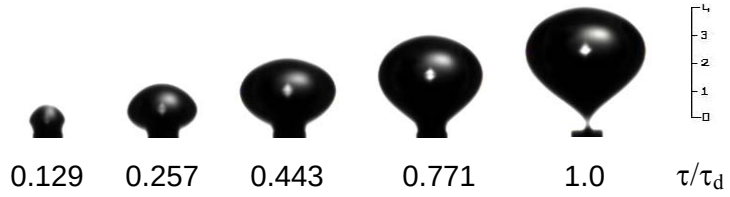

(b) d_o = 1.0 mm, d_b = 3.96 mm, τ_d = 143 ms

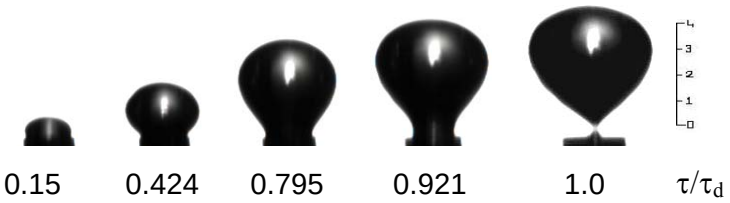

(c) d_o = 1.76 mm, d_b = 4.27mm, τ_d = 160 ms

Figure 3. Stages of bubble formation (nucleation to detachment) in water from different orifice sizes with an air-flow rate of 20 ml/min.

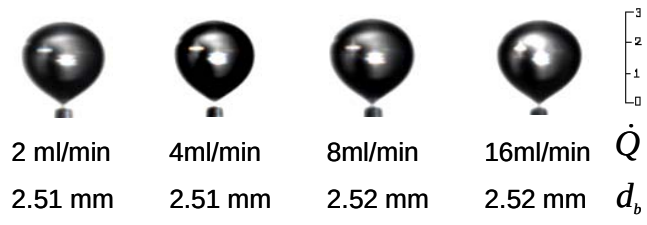

Figure 4. Flow-rate independent constant departure-bubble diameters – *static bubble regime* in water; d_o = 0.32 mm.

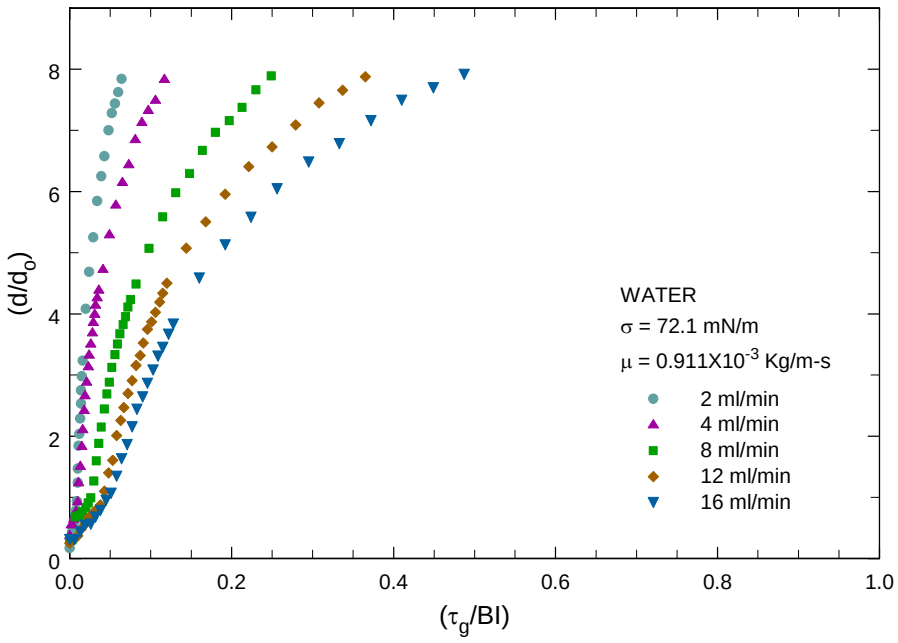

Figure 5. Temporal and spatial evolution in the *static bubble regime* in water with different air-flow rates and a capillary-tube orifice of d_o = 0.32 mm.

The interfacial properties of the liquid, particularly surface tension and viscosity, as would be expected from the force-balance depicted in Fig. 1, have a profound effect on the bubble dynamics. This is quantitatively depicted in Fig. 6, where the growth of single bubbles in four different liquids (ethanol, propylene glycol, water, and glycerol, which represent a spectrum of σ and μ values) are graphed. With an air flow rate of 12 ml/min through a 0.32-mm orifice in low σ ethanol, a smaller bubble is produced with almost negligible waiting time. In a pool of highly viscous glycerol, on the other hand, significantly larger bubbles with considerable waiting time (almost equal to the growth time) were produced as a result of higher viscous drag forces. A more balanced interplay of low σ and high μ, relative to water, is seen in the bubble evolution in propylene glycol. A comparative picture of departure size of bubbles generated in the four different liquids, as captured via high-speed digital videography, is presented in Fig. 7.

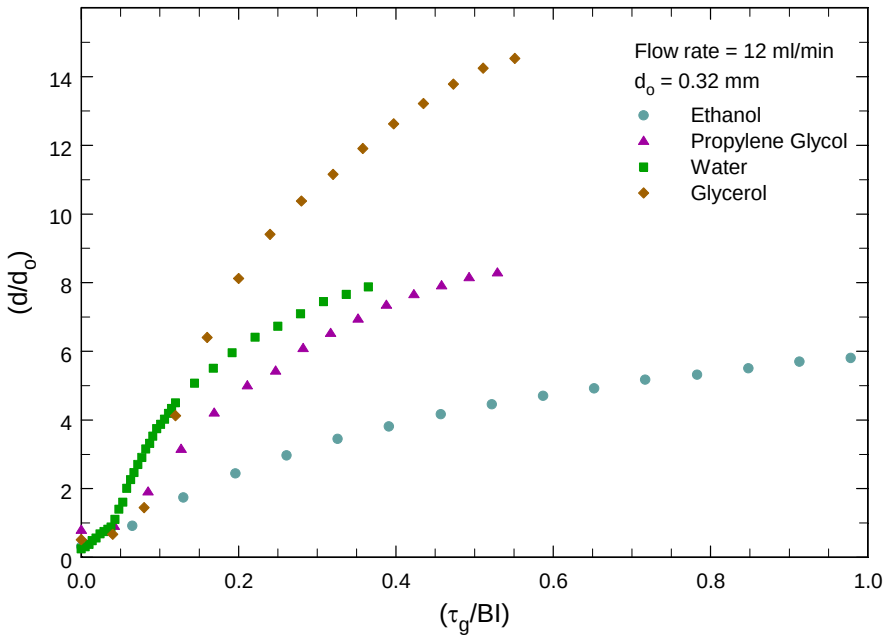

Figure 6. Temporal and spatial evolution in the *static bubble regime* with Q = 12 ml/min and d_o = 0.32 mm in different liquids.

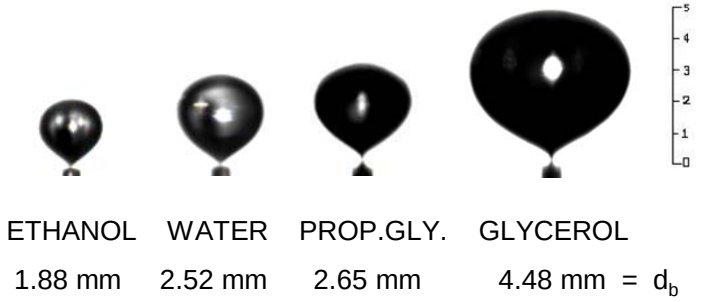

Figure 7. Departure bubble sizes in the *static bubble regime* with Q = 12 ml/min and d_o = 0.32 mm in different liquids.

The highest growth-time fraction of the bubble interval for ethanol (Fig. 6), which in turn implies a lower waiting time, can be attributed to its low surface tension characteristic. Ethanol has the lowest surface tension of the four liquids considered, and because in the initial stages of bubble formation, when the diameter is small, the predominant force that impedes bubble growth is due to surface tension, and hence its takes lesser time for the pressure force to overcome the

consequent resistance. This also explains the nearly zero initial slow-bubble-growth-regime for ethanol. The combined influence of σ and μ is seen the bubble-growth behavior in propylene glycol and glycerol with the same (τ_g/BI) fraction. Despite a lower surface tension, a relative high viscosity of propylene glycol and its restraining force lends to an almost equal initial slow-growth-regime for bubble evolution (~ 10% of BI) in the two liquids. Subsequently, however, the larger viscous drag effects of glycerol produce a substantially larger diameter bubble at departure.

The relative effect of orifice size on bubble formation in different fluids is illustrated in Fig. 8, where the spatial-temporal data for ebullience in water and glycerol with two different orifices (d_o = 0.32 and 1.76 mm) and air flow rate of 20 ml/min are graphed. An interesting feature is that while the departure bubble diameter is larger with a bigger orifice, (d/d_o) decreases in both fluids. The growth time to bubble interval fraction also decreases, suggesting a larger waiting time for bubble production in a larger orifice. This again is due to the dominance of surface tension forces in the early stages of bubble growth, and a larger pressure force is needed to overcome the initial resistance for the air-bubble embryo to be formed. As in the case of water (Fig. 5), in both ethanol and glycerol the decrease in waiting time and increase in growth-time to bubble-interval ratio with air flow rate is seen in Figs. 9 and 10. Also evident is constant d_b of the *static bubble regime* in the recorded ebullience in both low-σ ethanol and high-μ glycerol. Though not presented here, similar results were obtained in propylene glycol as well. The largest bubbles are formed in glycerol, which is the most viscous of the four fluids considered, whereas the smallest bubbles are produced in ethanol, which has the lowest surface tension; the departure-bubble sizes in water and propylene glycol lie within these two extremes.

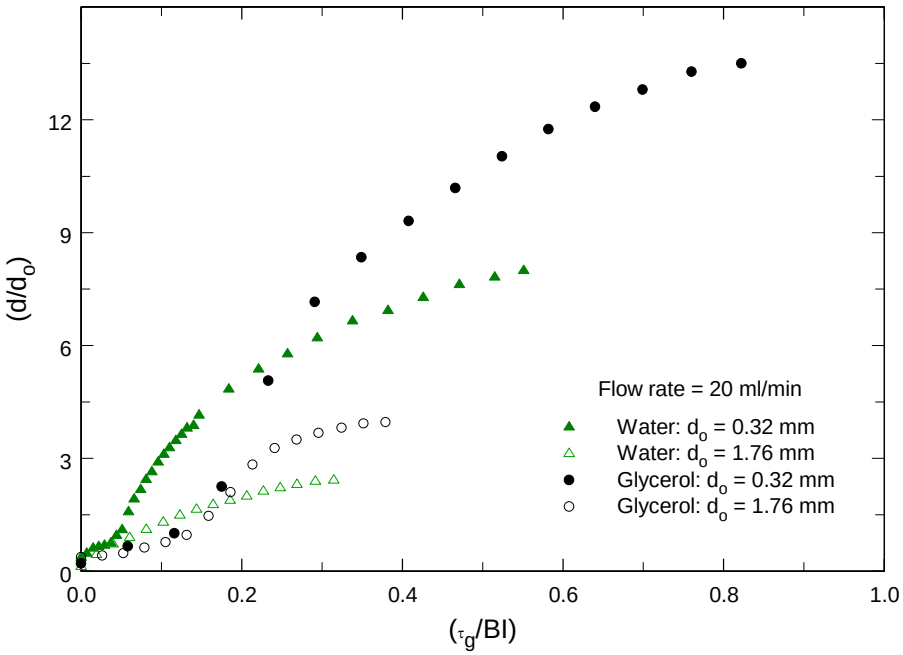

Figure 8. Effect of orifice diameter on bubble size and growth time in the *static bubble regime* with $\dot{Q}$ = 20 ml/min in water and glycerol.

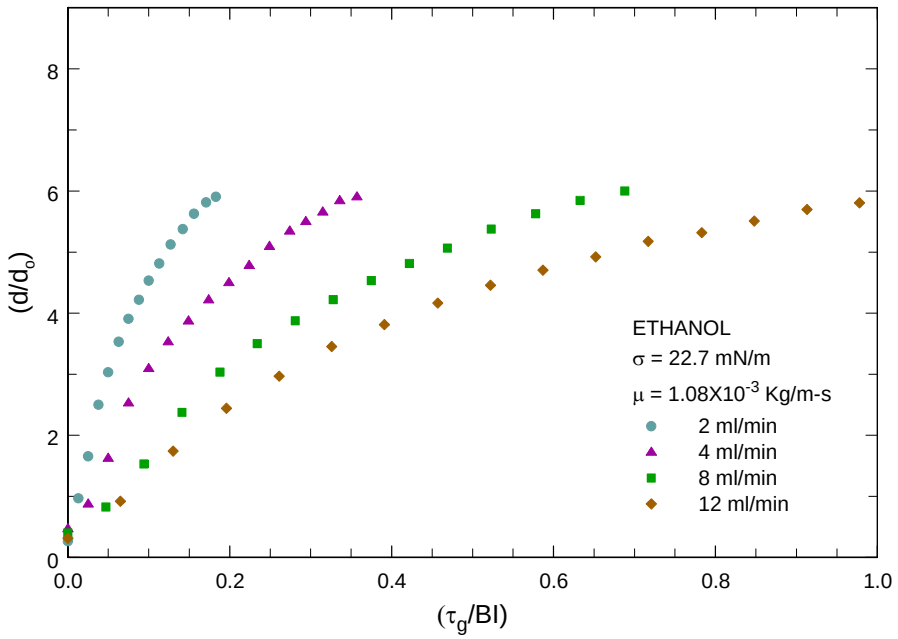

Figure 9. Temporal and spatial evolution in the *static bubble regime* in ethanol with different air-flow rates and a capillary-tube orifice of d_o = 0.32 mm.

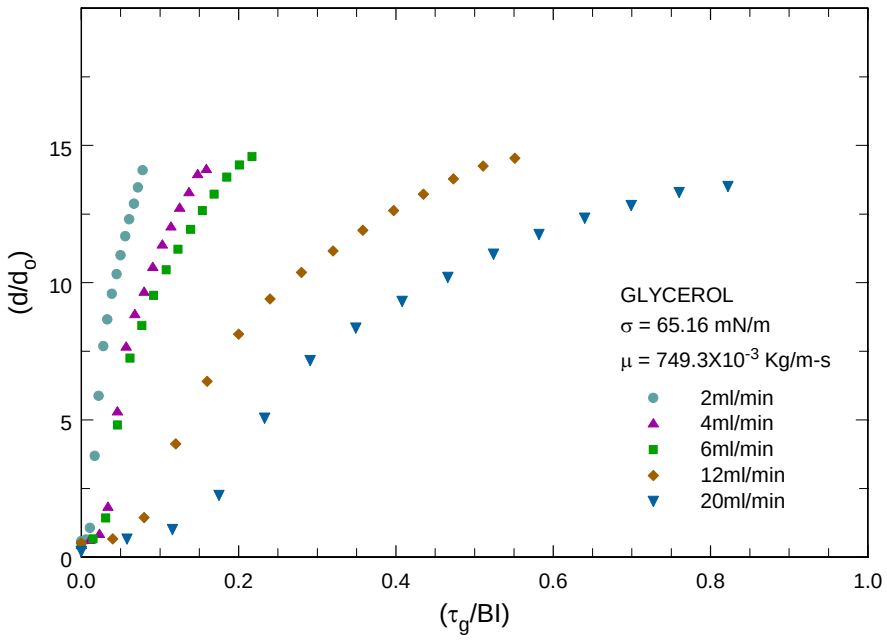

Figure 10. Temporal and spatial evolution in the *static bubble regime* in glycerol with different air-flow rates and a capillary-tube orifice of d_o = 0.32 mm.

The experimental data has also been compared with the predictions from the correlations proposed by Tadaki and Maeda [106] and Gaddis and Vogelpohl [110]. In both cases, when compared with typical data for water and d_o = 0.32 mm (Fig. 11), the bubble departure diameters are seen to be over predicted; the later correlation has considerably larger deviations particularly at higher flow rates. Also, contrary to the expectations, the Gaddis and Vogelpohl [110] predictions suggest a growing bubble diameter even when the air flow rate is essentially in the static regime. The results of a theoretical model developed by Kalaikadal et al. [112], based on a first-order balance of aiding and restraining forces depicted in Fig. 1, however, show an excellent agreement with experimental data in Fig. 11 for this case. Similar agreements are seen with data for other orifice sizes and fluids, and a limited set of such comparisons for air-water data of this study as well as those of others in the literature have been presented elsewhere [112]. A simple

dimensionless representation of the force balance suggests that the departure bubble diameter is functionally scaled as follows:

$$d_b \sim (d_o, L_c, \text{We}, \text{Bo}) \tag{7}$$

Devising an effective and generalized predictive correlation on the basis of this mechanistic scaling, and extending it over both the static and growing bubble regimes, is the subject of an extension of this study.

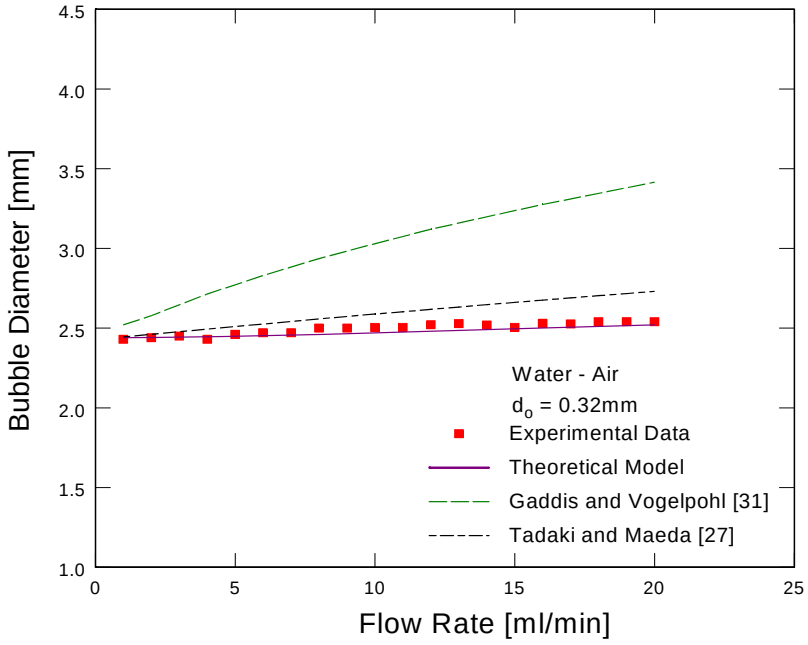

Figure 11. Comparison of present single-bubble (departure diameter d_b) data in the *static bubble regime* in a water-air system with predictions of correlations given by Tadaki and Maeda [106], and Gaddis and Vogelpohl [110].

Conclusions

The transient interfacial behavior of a growing bubble was experimentally observed to establish the determinants of ebullience in air-liquid systems. There exists a threshold value of flow rate below which the bubble diameter is constant (static bubble regime) which in turn is

unique for each orifice size. The single bubble formation in this regime is found to be dependent on the orifice size, and the surface tension and viscosity of the liquid; the latter two providing a rather complex interplay of controlling forces. In essence, for same flow rate, the departure bubble diameter increases with increase in the orifice diameter, surface tension and viscosity. A first-order phenomenological analysis suggests that d_b is scaled by the orifice diameter d_o, capillary length l_c, Weber number We, and Buoyancy number Bo.

Nomenclature

BI	bubble interval [ms]
d	diameter [mm]
d_b	bubble departure diameter [mm]
Fr	Froude number, $\left(V_g^2 / g d_o\right)$ [-]
g	acceleration due to gravity [m/s^2]
$\dot{Q}$	volumetric Flow Rate [ml/min]
Q_b	bubble volume [mm^3]
Re	Reynolds number, $(\rho_l V d_o / \mu_l)$ [-]
V_g	gas velocity [m/s]
We	Weber Number, $\left(\rho_l V_g^2 d_o / \rho_l\right)$ [-]
μ	viscosity [kg/m·s]
ρ	density [kg/m^3]
σ	surface tension [mN/m]
τ	time [ms]

Subscripts

b	bubble
d	at departure
g	gas and/or pertaining to growth
l	liquid
o	orifice

BIBLIOGRAPHY

[1] Manglik, R.M., Vishnubhatla, S.C., and Subramani, A., Interfacial Characterization of Aqueous Reagent Solutions, Technical Report TFTPL-DOE-NEER-Y2, University of Cincinnati, Cincinnati, OH, 2009.

[2] Manglik, R.M., Kalaikadal, D.S., Deodhar, A., and Subramani, A., Experimental Characterization of Bubble-Dynamics in Isothermal Liquid Pools, Technical Report TFTPL-DOE-NEER-Y3, University of Cincinnati, Cincinnati, OH, 2010.

[3] Bergles, A.E., Two-Phase Flow and Heat Transfer, 1756-1981, *Heat Transfer Engineering*, **2**(3-4), pp. 101-114, 1981.

[4] Nishikawa, K., Historical Developments in the Research of Boiling Heat Transfer, *JSME International Journal*, **30**(264), pp. 897-905, 1987.

[5] Manglik, R.M., On the Advancements in Boiling, Two-Phase Flow Heat Transfer, and Interfacial Phenomena, *Journal of Heat Transfer*, **128**(12), pp. 1237-1242, 2006.

[6] Manglik, R.M., and Jog, M.A., Molecular-to-Large-Scale Heat Transfer with Multiphase Interfaces: Current Status and New Directions, *Journal of Heat Transfer*, **131**(12), pp. 121001-1 - 121001-11, 2009.

[7] Bergles, A.E., Fundamentals of Boiling and Evaporation, *Two-Phase Flow Heat Exchangers: Thermal-Hydraulic Fundamentals and Design*, Ed. Kakaç, S., Bergles, A.E. and Fernandes, E.O., 159-200, Kluwer, The Netherlands, 1988.

[8] Dhir, V.K., Boiling Heat Transfer, *Annual Reviews of Fluid Mechanics*, **30**, pp. 365-401, 1998.

[9] Kenning, D.B.R., What do we Really Know about Nucleate Boiling, *IMechE Trans., 6th UK National Heat Transfer Conference, Edinburgh*, pp. 143-167, 1999.

[10] Carey, V.P., *Liquid-Vapor Phase-Change Phenomena*, Taylor & Francis, New York, NY, 2008.

[11] Hsu, Y.Y., On the Size of Range of Active Nucleation Cavities on a Heating Surface, *Journal of Heat Transfer*, **84**, pp. 207, 1962.

[12] Han, C.Y., and Griffith, P., The Mechanism of Heat Transfer in Nucleate Pool Boiling-Part I: Bubble Initiation, Growth and Departure, *International Journal of Heat and Mass Transfer*, **8**(6), pp. 887-904, 1965.

[13] Cooper, M.G., and Lloyd, A.J.P., The Microlayer in Nucleate Pool Boiling, *International Journal of Heat and Mass Transfer*, **12**(8), pp. 895-913, 1969.

[14] Dhir, V.K., Numerical Simulation of Pool-Boiling Heat Transfer, *AIChE Journal*, **47**(4), pp. 813-834, 2001.

[15] Singh, A., Mikiç, B.B., and Rohsenow, W.M., Active Sites in Boiling, *Journal of Heat Transfer*, **98**(3), pp. 401-406, 1976.

[16] Roy Chowdhury, S.K., and Winterton, R.H.S., Surface Effects in Pool Boiling, *International Journal of Heat and Mass Transfer*, **28**(10), pp. 1881-1889, 1985.

[17] Plesset, M.S., and Zwick, S.A., The Growth of Vapor Bubbles in Superheated Liquids, *Journal of Applied Physics*, **25**(4), pp. 493-500, 1954.

[18] Lay, J.H., and Dhir, V.K., Shape of a Vapor Stem During Nucleate Boiling of Saturated Liquids, *Journal of Heat Transfer*, **117**, pp. 394-401, 1995.

[19] Wasekar, V.M., and Manglik, R.M., Short-Time-Transient Surfactant Dynamics and Marangoni Convection around Boiling Nuclei, *Journal of Heat Transfer*, **125**(5), pp. 858-866, 2003.

[20] Shoji, M., Studies of Boiling Chaos: A Review, *International Journal of Heat and Mass Transfer*, **47**(6-7), pp. 1105-1128, 2004.

[21] Zhang, J., and Manglik, R.M., Nucleate Pool Boiling of Aqueous Polymer Solutions on a Cylindrical Heater, *Journal of Non-Newtonian Fluid Mechanics*, **125**(2-3), pp. 185-196, 2005.

[22] Sadhal, S.S., Ayyaswamy, P.S., and Chung, J.N., *Transport Phenomena with Drops and Bubbles*, Springer, New York, NY, 1997.

[23] Wasekar, V.M., and Manglik, R.M., Pool Boiling Heat Transfer in Aqueous Solutions of an Anionic Surfactant, *Journal of Heat Transfer*, **122**(4), pp. 708-715, 2000.

[24] Zhang, J., and Manglik, R.M., Effect of Ethoxylation and Molecular Weight of Cationic Surfactants on Nucleate Boiling in Aqueous Solutions, *Journal of Heat Transfer*, **126**(1), pp. 34-42, 2004.

[25] Zhang, J., and Manglik, R.M., Additive Adsorption and Interfacial Characteristics of Nucleate Pool Boiling in Aqueous Surfactant Solutions, *Journal of Heat Transfer*, **127**(7), pp. 684-691, 2005.

[26] Gatne, K.P., Jog, M.A., and Manglik, R.M., Surfactant-Induced Modification of Low Weber Number Droplet Impact Dynamics, *Langmuir*, **25**(14), pp. 8122-8130, 2009.

[27] Rosen, M.J., *Surfactants and Interfacial Phenomena*, 3rd Ed., Wiley-Interscience, Hoboken, NJ, 2004.

[28] Somasundaran, P., and Krishnakumar, S., Adsorption of Surfactants and Polymers at the Solid-Liquid Interface, *Colloids and Surfaces A: Physicochemical and Engineering Aspects*, **123-124**, pp. 491-513, 1997.

[29] Somasundaran, P., Simple Colloids in Simple Environments Explored in the Past, Complex Nanoids in Dynamic Systems to be Conquered Next: Some Enigmas, Challenges, and Strategies, *Journal of Colloid and Interface Science*, **256**(1), pp. 3-15, 2002.

[30] Fuerstenau, D.W., Equilibrium and Nonequilibrium Phenomena Associated with the Adsorption of Ionic Surfactants at Solid-Water Interfaces, *Journal of Colloid and Interface Science*, **256**(1), pp. 79-90, 2002.

[31] Wasan, D.T., and Nikolov, A.D., Spreading of Nanofluids on Solids, *Nature*, **423**, pp. 156-159, 2003.

[32] Chaudhury, M.K., Spread the Word about Nanofluids, *Nature*, **423**, pp. 131-132, 2003.

[33] Holmberg, K., Jönsson, B., Kronberg, B., and Lindman, B., *Surfactants and Polymers in Aqueous Solution*, Wiley, New York, NY, 2003.

[34] Manne, S., and Gaub, H.E., Molecular Organization of Surfactants at Solid-Liquid Interfaces, *Science*, **270**, pp. 1480-1483, 1995.

[35] Manglik, R.M., Wasekar, V.M. and Zhang, J., Dynamic and Equilibrium Surface Tension of Aqueous Surfactant and Polymeric Solutions, *Experimental Thermal and Fluid Science*, **25**(1-2), pp. 55-64, 2001.

[36] Hunter, R.J., *Foundations of Colloid Science*, Oxford University Press, Oxford, UK, 2001.

[37] Hoffmann, H., and Rehage, H., Rheology of Surfactant Solutions, *Surfactant Solutions - New Methods of Investigation*, Ed. Zana, R., 22, 209-239, Marcel Dekker, New York, NY, 1986.

[38] Carreau, P.J., De Kee, D.C.R., and Chhabra, R.P., *Rheology of Polymeric Systems: Principles and Applications*, Hanser Gardner Publications, New York, NY, 1997.

[39] Bird, R.B., Armstrong, R.C., and Hassager, O., *Dynamics of Polymeric Liquids: Vol. 1 - Fluid Mechanics*, Wiley, New York, NY, 1987.

[40] Hu, R.Y.Z., Wang, A.T.A., and Hartnett, J.P., Surface Tension Measurement of Aqueous Polymer Solutions, *Experimental Thermal and Fluid Science*, **4**(6), pp. 723-729, 1991.

[41] Fainerman, V.B., Makievski, A.V., and Miller, R., The Measurement of Dynamic Surface Tensions of Highly Viscous Liquids by the Maximum Bubble Pressure Method, *Colloids and Surfaces A: Physicochemical and Engineering Aspects*, **75**(1), pp. 229-235, 1993.

[42] Miller, R., Joos, P., and Fainerman, V.B., Dynamic Surface and Interfacial Tensions of Surfactant and Polymer Solutions, *Advances in Colloid and Interface Science*, **49**(1), pp. 249-302, 1994.

[43] Zhang, J., and Manglik, R.M., Experimental and Computational Study of Nucleate Pool Boiling Heat Transfer in Aqueous Surfactant and Polymer Solutions, Technical Report No. TFTPL-10, University of Cincinnati, Cincinnati, OH, 2004.

[44] Defay, R., and Petré, G., Dynamic Surface Tension, *Surface and Colloid Science*, Ed. Matijevic, E., 27-81, Wiley, New York, NY, 1971.

[45] Myers, D., *Surfaces, Interfaces, and Colloids*, 2nd Ed., Wiley-VCH, New York, NY, 1999.

[46] Razafindralambo, H., Blecker, C., Delhaye, S., and Paquot, M., Application of the Quasi-Static Mode of the Drop Volume Technique to the Determination of Fundamental Surfactant Properties, *Journal of Colloid and Interface Science*, **174**(2), pp. 373-377, 1995.

[47] Manglik, R.M., Jog, M.A., Subramani, A., and Gatne, K., Mili-Scale Visualization of Bubble Growth-Translation and Droplet Impact Dynamics, *Journal of Heat Transfer*, **128**(8), pp. 736, 2006.

[48] Persson, B., Nilsson, S., and Sundelöf, L.-O., On the Characterization Principles of Some Technically Important Water-Soluble Nonionic Cellulose Derivatives. Part II: Surface Tension and Interaction with a Surfactant, *Carbohydrate Polymers*, **29**(2), pp. 119-127, 1996.

[49] Levitz, P.E., Adsorption of Non Ionic Surfactants at the Solid/Water Interface, *Colloids and Surfaces A: Physicochemical and Engineering Aspects*, **205**(1-2), pp. 31-38, 2002.

[50] Miller, C.A., and Neogi, P., *Interfacial Phenomena: Equilibrium and Dynamic Effects*, Marcel Dekker, New York, NY, 1985.

[51] Wilson, M.D., and Whitesides, G.M., The Anthranilate Amide of "Polyethylene Carboxylic Acid" Shows an Exceptionally Large Change with pH in its Wettability by Water, *Journal of the American Chemical Society*, **110**(26), pp. 8718-8719, 1988.

[52] Hunter, R.J., *Zeta Potential in Colloid Science-Principles and Applications*, Academic Press, New York, NY, 1981.

[53] Evans, D.F., and Wennerström, H., *The Colloidal Domain - Where Physics, Chemistry, and Biology Meet*, Wiley-VCH, New York, NY, 1999.

[54] Kwok, D.Y., and Neumann, A.W., Contact Angle Measurement and Contact Angle Interpretation, *Advances in Colloid and Interface Science*, **81**(3), pp. 167-249, 1999.

[55] Wasekar, V.M., and Manglik, R.M., The Influence of Additive Molecular Weight and Ionic Nature on the Pool Boiling Performance of Aqueous Surfactant Solutions, *International Journal of Heat and Mass Transfer*, **45**(3), pp. 483-493, 2002.

[56] Bar-Cohen, A., Hysteresis Phenomena at the Onset of Nucleate Boiling, *Proc. of Pool and External Flow Boiling*, 1-14, ASME, New York, 1992.

[57] Kotchaphakdee, P., and Williams, M.C., Enhancement of Nucleate Pool Boiling with Polymeric Additives, *International Journal of Heat and Mass Transfer*, **13**(5), pp. 835-848, 1970.

[58] Levitskiy, S.P., Khusid, B.M., and Shul'man, Z.P., Growth of Vapor Bubbles in Boiling Polymer Solutions-II. Nucleate Boiling Heat Transfer, *International Journal of Heat and Mass Transfer*, **39**(3), pp. 639-644, 1996.

[59] Manglik, R.M., Bahl, M., Vishnubhatla, S., and Zhang, J., Interfacial and Rheological Characterization of Aqueous Surfactant and Polymer Solutions, TFTPL-9, University of Cincinnati, Cincinnati, OH, 2003.

[60] Zhang, J., and Manglik, R.M., Visualization of Ebullient Dynamics in Aqueous Surfactant Solutions, *Journal of Heat Transfer*, **125**(4), pp. 547, 2003.

[61] Bang, K.H., Kim, M.H., and Jeun, G.D., Boiling Characteristics of Dilute Polymer Solutions and Implications for the Suppression of Vapor Explosions, *Nuclear Engineering and Design*, **177**(1-3), pp. 255-264, 1997.

[62] Bergles, A.E., New Frontiers in Enhanced Heat Transfer, *Advances in Enhanced Heat Transfer*, Ed. Manglik, R.M., Ravigururajan, T.S., Muley, A., Papar, R.A., and Kim, J., HTD-Vol. 365, 1-8, ASME, New York, NY, 2000.

[63] Manglik, R.M., Heat Transfer Enhancement, *Heat Transfer Handbook*, Ed. Bejan, A., and Kraus, A.D., Chap. 14, Wiley, New York, NY, 2003.

[64] Wang, A.T.A., and Hartnett, J. P., Influence of Surfactants on Pool Boiling of Aqueous Polyacrylamide Solutions, *Wärme- und Stoffübertragung*, **27**(4), pp. 245-248, 1992.

[65] Paul, D.D., and Abdel-Khalik, S. I., Saturated Nucleate Pool Boiling Bubble Dynamics in Aqueous Drag-Reducing Polymer Solutions, *International Journal of Heat and Mass Transfer*, **27**(12), pp. 2426-2428, 1984.

[66] Yang, Y.M., and Maa, J. R., Effects of Polymer Additives on Pool Boiling Phenomena, *Letters in Heat and Mass Transfer*, **9**(4), pp. 237-244, 1982.

[67] Shul'man, Z.P., Khusid, B. M., and Levitskiy, S. P., Special Features of Boiling of Macromolecular Polymer Solutions, *Heat Transfer Research*, **25**(7), pp. 872-878, 1993.

[68] Chhabra, R.P., and Richardson, J.F., *Non-Newtonian Flow in the Process Industries: Fundamentals and Engineering Applications*, Butterworth-Heinemann, Oxford, UK, 1999.

[69] Athavale, A.D., Characterization Of Nucleate Pool Boiling Heat Transfer Of Aqueous Polymeric Solutions, M.S., University of Cincinnati, Cincinnati, OH, 2011.

[70] Jung, C., and Bergles, A.E., Evaluation of Commercial Enhanced Tubes in Pool Boiling, Technical Report No. DE-FC07-88ID 12772, Rensselaer Polytechnic Institute, Troy, NY, 1989.

[71] Wasekar, V.M., and Manglik, R.M., Nucleate Pool Boiling Heat Transfer in Aqueous Surfactant Solutions, Technical Report No. TFTPL-4, University of Cincinnati, Cincinnati, OH, 2001.

[72] Moffatt, R.J., Describing the Uncertainties in Experimental Results, *Experimental Thermal and Fluid Science*, **1**(1), pp. 3-17, 1988.

[73] Rohsenow, W.M., A Method of Correlating Heat Transfer Data for Surface Boiling of Liquids, *Transactions of the ASME*, **74**(3), pp. 969-976, 1952.

[74] Borishanskii, V.M., Correlation of the Effect of Pressure on the Critical Heat Flux and Heat Transfer Rates Using the Theory of Thermodynamic Similarity, *Problems of Heat Transfer and Hydraulics of Two-Phase Media*, Ed. Kutateladze, S.S., 16-37, Pergamon Press, New York, NY, 1969.

[75] Cooper, M.G., Saturated Nucleate Pool Boiling - A Simple Correlation, *Proc. of First U.K. National Conference on Heat Transfer*, **2**, 785-793, Institute of Chemical Engineers, University of Leeds, UK, 1984.

[76] Cornwell, K., and Houston, S.D., Nucleate Pool Boiling on Horizontal Tubes: A Convection-Based Correlation, *International Journal of Heat and Mass Transfer*, **37**(Supl. 1), pp. 303-309, 1994.

[77] Hiemenz, P.C., *Polymer Chemistry: The Basic Concepts*, Marcel Dekker, New York, NY, 1984.

[78] Macosko, C.W., *Rheology: Principles, Measurements, and Applications*, Wiley, New York, NY, 1994.

[79] Cross, M.M., Rheology of Non-Newtonian Fluids: A New Flow Equation for Pseudoplastic Systems, *Journal of Colloid Science*, **20**(5), pp. 417-437, 1965.

[80] Soong, D., and Shen, M., Shear-Rate-Dependent Viscosity of Non-Newtonian Suspensions and Entangled Polymer Systems, *Polymer Engineering and Science*, **20**(17), pp. 1177-1180, 1980.

[81] Castelain, C., Doublier, J. L., and Lefebvre, J., A Study of the Viscosity of Cellulose Derivatives in Aqueous Solutions, *Carbohydrate Polymers*, **7**(1), pp. 1-16, 1987.

[82] Dunleavy, J.E., and Middleman, S., Correlation of Shear Behavior of Solutions of Polyisobutylene, *Journal of Rheology*, **10**(1), pp. 157-168, 1966.

[83] Hiemenz, P.C., and Rajagopalan, R., *Principles of Colloid and Surface Chemistry*, 3rd Ed., Marcel Dekker, New York, NY, 1997.

[84] Ibrahim, F.W., Correct Determination of Staudinger's Index (Intrinsic Viscosity) and of Huggins' Constant, *Journal of Polymer Science, Part A: General Papers*, **3**(2), pp. 469-478, 1965.

[85] De Gennes, P., *Scaling Concepts in Polymer Physics*, Cornell University Press, Ithaca, NY, 1979.

[86] Foroutan, M., Khoee, S., and Zarrabi, M., Overlap Concentration of an Aqueous Poly(N-vinylcaprolactam) Solution in the Dynamic and Static States, *Journal of Applied Polymer Science*, **109**(1), pp. 597-601, 2008.

[87] Broseta, D., Leibler, L., Lapp, A., and Strazielle, C., Universal Properties of Semi-Dilute Polymer Solutions: A Comparison between Experiments and Theory, *Europhysics Letters*, **2**(9), pp. 733-737, 1986.

[88] Cosgrove, T., and Griffiths, P. C., The Critical Overlap Concentration Measured by Pulsed Field Gradient Nuclear Magnetic Resonance Technique, *Polymer*, **35**(3), pp. 509-513, 1994.

[89] Hua, X.Y., and Rosen, M.J., Dynamic Surface Tension of Aqueous Surfactant Solutions. I. Basic Parameters, *Journal of Colloid and Interface Science*, **124**(2), pp. 652-659, 1988.

[90] Lee, K.S., Ivanova, N., Starov, V. M., Hilal, N., and Dutschk, V., Kinetics of Wetting and Spreading by Aqueous Surfactant Solutions, *Advances in Colloid and Interface Science*, **144**(1-2), pp. 54-65, 2008.

[91] Thome, J.R., *Enhanced Boiling Heat Transfer*, Hemisphere, New York, NY, 1990.

[92] Bergles, A.E., Enhancement of Pool Boiling, *International Journal of Refrigeration*, **20**(8), pp. 545-551, 1997.

[93] Wasekar, V.M., and Manglik, R.M., A Review of Enhanced Heat Transfer in Nucleate Pool Boiling of Aqueous Surfactant and Polymeric Solutions, *Journal of Enhanced Heat Transfer*, **6**(2-4), pp. 135-150, 1999.

[94] Wu, W., Yang, Y., and Maa, J., Nucleate Pool Boiling Enhancement by Means of Surfactant Additives, *Experimental Thermal and Fluid Science*, **18**(3), pp. 195-209, 1998.

[95] Ammerman, C.N., and You, S.M., Determination of Boiling Enhancement Mechanism Caused by Syrfactant Addition to Water, *Journal of Heat Transfer*, **118**(2), pp. 429-435, 1996.

[96] Kulkarni, A.A., and Joshi, J.B., Bubble Formation and Bubble Rise Velocity in Gas-Liquid Systems: A Review, *Industrial and Engineering Chemistry Research*, **44**(16), pp. 5873-5931, 2005.

[97] Hughes, R.R., Handlos, A.E., Evans, H.D., and Maycock, R.L., The Formation of Bubbles at Simple Orifices, *Chemical Engineering Progress*, **51**(12), pp. 557-563, 1955.

[98] Eversole, W.G., Wagner, G.H., and Stackhouse, E., Rapid Formation of Gas Bubbles in Liquids, *Industrial and Engineering Chemistry*, **33**(11), pp. 1459-1462, 1941.

[99] van Krevelen, D.W., and Hoftijzer, P.J., Studies of Gas-Bubble Formation: Calculation of Interfacial Area in Bubble Contactors, *Chemical Engineering Progress*, **46**(1), pp. 29-35, 1950.

[100] Tate, T., On the Magnitude of a Drop of Liquid Formed Under Different Circumstances, *Philosophical Magazine*, **27**(181), pp. 176-180, 1864.

[101] Datta, R.L., Napier, D.H., and Newitt, D.M., The Properties and Behavior of Gas Bubbles Formed at a Circular Orifice, *Proc. of Conference on Formation and Properties of Gas Bubbles*, 14-26, IChemE, London, UK, 1950.

[102] Benzing, R.J., and Myers, J.E., Low Frequency Bubble Formation at Horizontal Circular Orifices, *Industrial and Engineering Chemistry*, **47**(10), pp. 2087-2090, 1955.

[103] Davidson, L., and Amick, E.H., Formation of Gas Bubbles at Horizontal Orifices, *AIChE Journal*, **2**(3), pp. 337-342, 1956.

[104] Calderbank, P.H., Gas-Liquid Contacting on Plates, *Transactions of the Institution of Chemical Engineers*, **34**, pp. 79-90, 1956.

[105] Davidson, J.F., and Schüler, O.G., Bubble Formation at an Orifice in an Inviscid Liquid, *Transactions of the Institution of Chemical Engineers*, **38**, pp. 335-342, 1960.

[106] Tadaki, T., and Maeda, S., The Size of Bubbles from Single Orifices, *Kagaku Kogaku*, **1**(1), pp. 55-60, 1963.

[107] Kupferberg, A., and Jameson, G.J., Bubble Formation at a Submerged Orifice above a Gas Chamber of Finite Volume, *Transactions of the Institution of Chemical Engineers*, **47**, pp. T241-T250, 1969.

[108] Wraith, A.E., Two Stage Bubble Growth at a Submerged Plate Orifice, *Chemical Engineering Science*, **26**, pp. 1659-1671, 1971.

[109] Räbiger, *VDI-Forschungsheft*, **625**, 1984.

[110] Gaddis, E.S., and Vogelpohl, A., Bubble Formation in Quiescent Liquids under Constant Flow Conditions, *Chemical Engineering Science*, **41**(1), pp. 97-105, 1986.

[111] Kumar, R., and Kuloor, N.R., The Foundation of Bubbles and Drops, *Advances in Chemical Engineering*, Ed. 8, Academic Press, New York, NY, 1970.

[112] Kalaikadal, D.S., Kasimsetty, S.K., and Manglik, R.M., A Theoretical Model for Gas-Bubble Growth at a Submerged Capillary-Tube Orifice Tip in Quiescent Liquid Pools, *Chemical Engineering Science*, **X**(being submitted), pp. 1-10, 2011.